Phase space optimization of quantum representations: Direct-product basis sets

Bill Poirier[a] and J. C. Light
The James Franck Institute, The University of Chicago, Chicago, Illinois 60637

(Received 11 March 1999; accepted 18 June 1999)

The quantitative phase space similarities between the uniformly mixed ensembles of eigenstates, and the quasiclassical Thomas–Fermi distribution, are exploited in order to generate a nearly optimal basis representation for an arbitrary quantum system. An exact quantum optimization functional is provided, and the minimum of the corresponding quasiclassical functional is proposed as an excellent approximation in the limit of large basis size. In particular, we derive a stationarity condition for the quasiclassical solution under the constraint of strong separability. The corresponding quantum result is the phase space optimized direct-product basis—customized with respect to the Hamiltonian itself, as well as the maximum energy of interest. For numerical implementations, an iterative, self-consistent-field-like algorithm based on optimal separable basis theory is suggested, typically requiring only a few reduced-dimensional integrals of the potential. Results are obtained for a coupled oscillator system, and also for the 2D Henon–Heiles system. In the latter case, a phase space optimized discrete variable representation (DVR) is used to calculate energy eigenvalues. Errors are reduced by several orders of magnitude, in comparison with an optimized sinc-function DVR of comparable size. © *1999 American Institute of Physics*. [S0021-9606(99)00235-4]

I. INTRODUCTION

With each passing year, experimentalists and theorists are gathering increasingly accurate and specific data, on successively larger polyatomic systems, at higher and higher energies. For the theorists among us who calculate energy eigenspectra and the like, one fact has become very clear: the choice of representation has a *crucial* effect on the efficiency of the calculation. In all but the simplest applications, one attempts to incorporate at least some of the underlying physics into the representational basis itself—perhaps via a harmonic expansion about some equilibrium geometry, for example. However, for many polyatomic systems and energy regimes of current interest, the harmonic picture is simply no longer very helpful. Anharmonicity of the potential is one widely recognized cause; but for multidimensional systems at higher energies, nonseparability is probably an even greater culprit.[1] In any event, a more sophisticated physical picture is evidently required, both from a pedagogical standpoint, and also from the practical perspective of improving computational efficiency.

The primary goal of this paper is to optimize the basis representation for a particular system—with respect to the efficiency of the subsequent numerical computation—in as general and rigorous a manner as possible. It is also hoped that the resultant optimal basis may provide some physical insight into the underlying system; but computational efficiency is, in any event, the principal criterion for success. Ideally, an optimization of this sort could be tailored to both the system itself and the energy range of interest—for the latter has a great impact upon the efficiency. Moreover, since all computations are finite, it would be desirable to take the basis size into account as well. Another extremely valuable feature would be some quantitative measure of the method's anticipated success in specific applications. This is important because it would enable one to distinguish the truly optimal representations from those that are merely ''improved.'' Finally, it should be permissible to constrain the basis functions, in whatever manner is appropriate for the computational method being used.

The direct-product basis sets (DPBs)[2,3] for instance, also known as ''strongly separable bases,''[4] comprise the focus of this paper. There is an inherent significance to these representations—consisting, as they do, of functions which are separable products in the coordinates. But our interest in direct products also stems from their being the appropriate constraint for the discrete variable representation (DVR) grid methodology.[5–10] As it happens, there is already a general framework for improving the efficiency of DPB representations, known as the ''potential-optimized DVR'' (PO DVR).[11,12] The general idea is to exploit the properties of the true potential in the determination of the one-dimensional marginal wave functions whose multidimensional products comprise the basis. In an inelastic scattering problem, for instance, the asymptotic form of the true potential may, by virtue of its separability, divide naturally into ''effective'' 1D potentials for each of the various degrees of freedom. By using these effective potentials to define the basis set for each degree of freedom, one can obtain a DPB—and corresponding DVR—that is tailored for the particular system at hand.

Such is the promise of the PO DVR approach. However, the success of this method in practice hinges on two key

[a]Electronic mail: billp@rainbow.uchicago.edu

factors: the particular procedure that is used to obtain the effective 1D potentials from the true multidimensional potential; and the choice of coordinates itself. The latter is presumed fixed for our purposes—although a coordinate transformation that renders the Hamiltonian more nearly separable might, in general, significantly improve matters. As for the former, various procedures have been proposed in the past, and have met with considerable success in certain applications.[13–15] What has been lacking however, is a general, systematic means of evaluating the efficiency of these procedures *a priori*. It turns out that a simple, yet rigorous quantum-mechanical functional for measuring representational efficiency does, in fact, exist [Eq. (2.8)]. Moreover, minimization of this functional yields the particular DPB which is truly ''optimized'' with respect to the potential, in the sense that there are no DPBs of comparable size which yield more accurate eigenvalues. In mathematical terms, this optimization is a variational quantum mechanics problem—essentially a generalization of the standard variational principle.

The exact quantum minimization is in general a difficult task, although it has been applied previously in a limited context.[8] Recently, however, it has been found that there is a corresponding *quasiclassical* optimization problem [Eq. (2.12)] whose solution is almost trivial. The heart of the argument lies in the fact that any finite basis set in quantum mechanics is represented approximately by some region in phase space of finite volume. This region can be interpreted as a kind of Thomas–Fermi distribution.[16–21] Moreover, using the correspondence rule developed by Weyl and Wigner,[22–25] we can make a quantitative comparison with the exact quantum result directly on phase space. One finds that the quasiclassical approximation is not very accurate for individual pure states, but that the correspondence becomes exceedingly accurate as the number of basis functions becomes large—even more so than a semiclassical approximation. This is, of course, precisely the limit in which the quantum problem becomes difficult, and for which an accurate approximation is desired.

We therefore advocate the use of the quasiclassical minimum—or some good approximation thereof—to generate a nearly optimal DPB for the representation. In DVR applications, the resultant grid is expected to require fewer points than for any other PO DVR treatment. Exactly how few still depends on the specifics of the system, of course. However, some indication is evident in Fig. 1(a), a plot of DVR grid points for a particularly troublesome potential with a localized ''hole'' in one small region. This kind of situation—which occurs quite frequently in real molecules[26]—is notoriously difficult for a standard sinc-function (sinc) DVR treatment, because the high density of points required to adequately represent the range of momenta in the hole must be extended throughout the entire configuration space. As is evident from Fig. 1 however, this difficulty is largely circumvented by the phase space optimized (PSO) DVR.

It is instructive to compare the present PSO approach with related optimization methods that have been used in the past. The PSO quantum functional is very similar to that of optimal separable basis (OSB) theory,[4,27,28] though the latter does not provide for optimization of the finite projection subspace. In general, finite projections are related to the first-order reduced density matrices of density functional theory. These density matrices have been previously exploited to perform a one-parameter optimization of hybrid orbitals.[29] The vibrational self-consistent field (VSCF) method,[1,30,31] however, is more closely related to the PSO approach—owing to the connection between the Hartree and OSB stationarity conditions.[4] Both methods yield separable basis functions—but the VSCF functions are not mutually orthogonal, and cannot be collectively optimized for a desired energy range. Another difference is that the VSCF optimization is quantum mechanical rather than quasiclassical, although a semiclassical VSCF method has been developed.[32] For grid or DVR applications, a 1D phase space optimization technique known as the ''mapped Fourier grid'' method has recently been introduced.[33,34]

The remainder of the paper is organized as follows. A

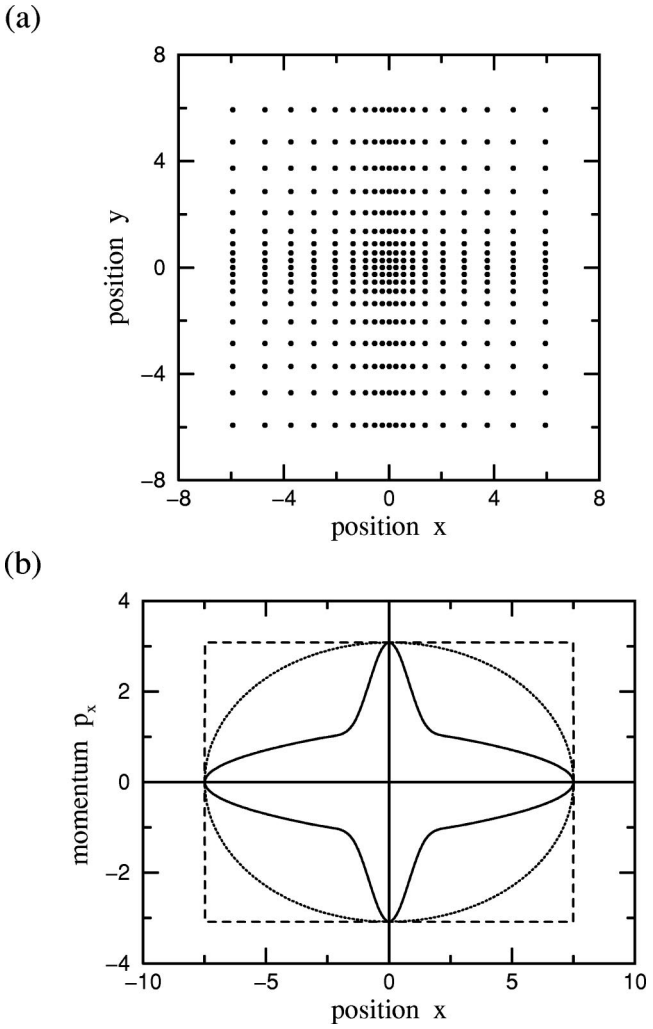

FIG. 1. Zeroth-order phase space optimization of $H=(p_x^2+p_y^2)/2+(r^2-4)e^{-r^2}+|r|/10$, with $r^2=x^2+y^2$ and maximum energy $E_{\max}^{(0)}=0.75$. There is a localized potential ''hole'' near the origin. (a) PSO DVR grid points are dense in the hole region, but sparse elsewhere. (b) Marginal phase space required by: sinc DVR (dashed); Gauss–Hermite DVR (dotted); PSO DVR (solid). Areas outside the solid curve result in extraneous points.

review of the pertinent theory is presented in Sec. II, including OSB theory (Sec. II A) and the quantum–quasiclassical correspondence on phase space (Sec. II B). In addition, the functionals of Eqs. (2.8) and (2.12) are derived, as is a simple *a priori* estimate of basis efficiency (Sec. II C). Section III focuses on the DPB problem, culminating in the stationarity condition for the exact quasiclassical solution (Sec. III B). An iterative algorithm suitable for computational applications is also presented (Sec. III C), and applied to DVRs (Sec. III D). In Sec. IV, the exact quasiclassical direct-product solutions for both the coupled and uncoupled harmonic oscillator systems are derived analytically, and shown to correspond to the exact quantum solutions. In Sec. V, we apply all of the previous ideas to the 2D Henon–Heiles system. The PSO potentials are obtained numerically (Sec. V B), compared with another standard choice,[15,35] and utilized in the calculation of the PSO DPB (Sec. V C). Finally, in Sec. V D, the PSO DVR is constructed—both with and without grid truncation—and a subsequent eigenvalue calculation performed. The accuracy of the results is compared with that of an optimized sinc DVR, where the number of grid points is the same in both cases.

II. THEORETICAL BACKGROUND

A. Optimal representations

Let $\hat{H}$ be a quantum Hamiltonian. In this section, we consider only kinetic-plus-potential $(T+V)$ Hamiltonians with two degrees of freedom:

$$\hat{H}=\frac{\hat{p}_x^2}{2m}+\frac{\hat{p}_y^2}{2m}+V(\hat{x},\hat{y}). \tag{2.1}$$

The dimensional units are such that products of canonically conjugate pairs such as xp_x have units of reduced Planck's constant—implying that $\hbar=1$, as is presumed throughout this work. The generalization to arbitrary dimensionality n, considered in the later sections, is for the most part straightforward.

The eigenstates of $\hat{H}$ are not, in general, direct-product functions in x and y. We are nevertheless interested in finding the best direct-product basis set (DPB) in which to represent $\hat{H}$. One approach is that of optimal separable basis (OSB) theory, which provides the best separable approximation $\hat{H}_0$ to the true Hamiltonian $\hat{H}$.[4,27,28] More specifically, $\hat{H}_0$ is chosen so as to minimize

$$\mathrm{tr}[(\hat{H}-\hat{H}_0)^2], \tag{2.2}$$

where the selection of $\hat{H}_0$ is made from the set of all possible Hermitian operators, subject to a suitable separability constraint.

Of the various constraints which one might consider,[4] the strongly separable constraint is appropriate here; this is because $\hat{H}_0$ then takes the form

$$\hat{H}_0=H_x(\hat{x},\hat{p}_x)+H_y(\hat{y},\hat{p}_y), \tag{2.3}$$

whose eigenstates must necessarily comprise a DPB. In Eq. (2.3), the 1D[36] operators $\hat{H}_x$ and $\hat{H}_y$ are known as ''marginal Hamiltonians.'' The constraint of Eq. (2.3) is more restrictive than other forms of separability which have been utilized in previous applications.[27,28] On the other hand, an analytical determination of the variational minimum is readily available.

Using Eqs. (2.1)–(2.3) and the variational calculus, the optimal strongly separable $\hat{H}_0$ can be shown to be

$$\hat{H}_x=\frac{\hat{p}_x^2}{2m}+V_x(\hat{x}), \quad \hat{H}_y=\frac{\hat{p}_y^2}{2m}+V_y(\hat{y}), \tag{2.4}$$

$$V_x(x)=\frac{\int V(x,y)\,dy}{\int dy}-\frac{1}{2}\langle V\rangle,$$
$$V_y(y)=\frac{\int V(x,y)\,dx}{\int dx}-\frac{1}{2}\langle V\rangle, \tag{2.5}$$

at least in principle—as is easily verified by adding an arbitrary strongly separable perturbation to $\hat{H}_0$, and evaluating Eq. (2.2) in configuration space. [$\langle V\rangle$ is the expectation value $\int V(x,y)\,dx\,dy/\int dx\,dy$, and it is assumed that $\min[V(x,y)]=0$.] In practice however, the right-hand sides of Eq. (2.5) may diverge, because the coordinate and energy limits are unrestricted.

For real-world applications, it is appropriate to introduce restrictions, because there is always a maximum energy or basis size of interest. This is most naturally accomplished by working with the projection of $\hat{H}$ on to a truncated set of basis functions $|\phi_i\rangle$ of finite size N. The projected Hamiltonian is

$$\hat{H}_{\mathrm{pr}}=\hat{\rho}_N\hat{H}\hat{\rho}_N, \tag{2.6}$$

whose representation in the $|\phi_i\rangle$ basis is an $N\times N$ matrix known as the ''variational basis representation'' (VBR).[8,9] The density operator $\hat{\rho}_N$ in Eq. (2.6) is a uniformly mixed ensemble (UME) of the truncated basis set wave functions:

$$\hat{\rho}_N\equiv\sum_{i=1}^{N}|\phi_i\rangle\langle\phi_i|. \tag{2.7}$$

Note that $\hat{\rho}_N$ is invariant with respect to unitary transformations of the N vectors $|\phi_i\rangle$. Formally, $\hat{\rho}_N$ represents the N-dimensional subspace spanned by those vectors, in the infinite-dimensional quantum Hilbert space. The $|\phi_i\rangle$'s are in principle arbitrary, but in practice are taken to be the lowest N eigenstates of some Hamiltonian-like operator.

For our purposes, the subspace $\hat{\rho}_N$ of the projected Hamiltonian is itself allowed to vary during the optimization; and in this crucial and complicating respect, the situation is quite different from that leading to Eqs. (2.4) and (2.5). It is in fact necessary to specify a new optimization criterion. A natural procedure—consistent with the general OSB approach—is to minimize the total discrepancy between the eigenvalues of $\hat{H}_{\mathrm{pr}}$ and $\hat{H}$. If we focus on the *lowest N* eigenvalues of $\hat{H}$, then the best choice of $\hat{\rho}_N$ is evidently that which minimizes $\mathrm{tr}(\hat{H}_{\mathrm{pr}})$—or equivalently,

$$\delta\,\mathrm{tr}(\hat{\rho}_N\hat{H})=0 \tag{2.8}$$

for all appropriate variations of $\hat{\rho}_N$. In practice, one is often interested in divorcing the number of desired eigenvalues K

from the basis size $N \geqslant K$, in which case the trace of Eq. (2.8) is replaced with the sum of the lowest K projected eigenvalues.

If $\hat{\rho}_N$ were allowed to be completely arbitrary [apart from satisfying Eq. (2.7)], then Eq. (2.8) would obviously yield perfect results, in that the optimal $|\phi_i\rangle$ would consist of the true eigenfunctions of $\hat{H}$, and the eigenvalues of $\hat{H}_{\rm pr}$ would match the first N eigenvalues of $\hat{H}$ exactly. For the scope of this paper however, $\hat{\rho}_N$ is *constrained* to be a finite DPB, so that the resultant stationary solution of Eq. (2.8) yields only approximate eigenvalues of $\hat{H}$—albeit the best such approximation possible. Even with these constraints in place, however, obtaining the quantum solution is generally nontrivial, because an infinite-dimensional variation on the Hilbert space is still required to locate the extremum. In its stead, we will solve the corresponding constrained quasiclassical problem.

B. Quasiclassical approximation on phase space

It is convenient to reexpress the quantum problem in the exact phase space representation of Wigner and Weyl. This formalism provides a unique correspondence between quantum-mechanical operators, and observables on a classical-like phase space.[22–25] The Hamiltonian of Eq. (2.1), for instance, is mapped to the phase space function $H=(p_x^2+p_y^2)/(2m)+V(x,y)$. The UME density operator $\hat{\rho}_N$ also has a unique representation $\rho_N^{\rm qm}(x,p_x,y,p_y)$, although the transformation here is far less trivial. In any event, it can be shown[25] that the trace in Eq. (2.8) becomes

$$\mathrm{tr}(\hat{\rho}_N \hat{H}) = (2\pi)^{-2} \int \rho_N^{\rm qm}(x,p_x,y,p_y) \times H(x,p_x,y,p_y)\, dx\, dp_x\, dy\, dp_y \tag{2.9}$$

under the Wigner–Weyl correspondence.

Equation (2.9) is exact, but difficult to evaluate in practice, because obtaining $\rho_N^{\rm qm}(x,p_x,y,p_y)$ is nontrivial. If $\hat{\rho}_N$ consists of the lowest N eigenstates of some operator $\hat{H}_0$ however—as is appropriate here—then an excellent quasiclassical approximation $\rho(x,p_x,y,p_y)$ is readily available:[19–21]

$$\rho(x,p_x,y,p_y) = \Theta(E_{\max} - H_0(x,p_x,y,p_y)), \tag{2.10}$$

where $H_0(x,p_x,y,p_y)$ is itself obtained from $\hat{H}_0$ via the Wigner–Weyl correspondence, and $E_{\max}$ is such that the enclosed phase space volume is equal to $(2\pi)^2 N$. Equation (2.10) can be regarded as a Thomas–Fermi phase space distribution. Note that $\hat{H}_0$ is *not* equivalent to $\hat{H}$: the former is not constrained to the $T+V$ form of Eq. (2.1), and moreover, varies during the optimization in accord with varying $\hat{\rho}_N$.

It would perhaps be more accurate to refer to the $\rho(x,p_x,y,p_y)$ of Eq. (2.10) as $\rho_{\hat{H}_0;N}^{\rm qc}(x,p_x,y,p_y)$, to indicate its quasiclassical nature and explicit dependence on $\hat{H}_0$ and N. We use the former notation, however, to avoid an awkward proliferation of sub(super)scripts. In any event, $\rho(x,p_x,y,p_y)$ is easy to obtain in practice, has a simple and intuitive phase space interpretation, satisfies the same algebraic properties as $\hat{\rho}_N$, and—most importantly—converges to the exact $\rho_N^{\rm qm}(x,p_x,y,p_y)$ in the large N limit. In the 1D case, individual eigenstates of $\hat{H}_0$ correspond quasiclassically to solid rings of area 2π—adjacent and nonoverlapping—whose boundaries occur along the contours of $H_0(x,p_x)$. In a very literal sense therefore, Eq. (2.10) is a classical ''uniformly mixed ensemble,'' albeit a 2D one. It can be convenient to interpret Eq. (2.10) not as a density, but simply as a *region* of phase space, which we shall refer to as $\mathcal{R}$. One might even generalize Eq. (2.10) by allowing *any* phase space region of volume $(2\pi)^2 N$ to approximate quasiclassically some quantum UME of N basis functions. An underlying $\hat{H}_0$ operator must be specified however, if this correspondence is to be unique.

The quantum distribution $\rho_N^{\rm qm}(x,p_x,y,p_y)$ tends to oscillate slightly about the quasiclassical $\rho(x,p_x,y,p_y)$, although the integrals over phase space are the same. This situation is not surprising, and has in fact already been thoroughly investigated in configuration space; for it can be shown that the projected density

$$\rho^q(x,y) = (2\pi)^{-2} \int \rho(x,p_x,y,p_y)\, dp_x\, dp_y \tag{2.11}$$

is mathematically equivalent to the standard Thomas–Fermi density for a collection of N noninteracting fermions described by $\hat{H}_0$.[19,21] In any event, the oscillatory behavior suggests that the quasiclassical approximation to $\mathrm{tr}(\hat{\rho}_N \hat{H})$—obtained by replacing $\rho_N^{\rm qm}(x,p_x,y,p_y)$ with $\rho(x,p_x,y,p_y)$ in the integral of Eq. (2.9)—should be quite accurate. We expect this to be the case even for relatively small N, because the integrand is a smoothly varying quantity which is fully integrated over all phase space coordinates.

The strategy therefore, is to minimize the quasiclassical approximation to $\mathrm{tr}(\hat{\rho}_N \hat{H})$, and to use the results to obtain the PSO DPB for representing $\hat{H}$. The quasiclassical analog of Eq. (2.8) (generalized for arbitrary dimensionality n) is as follows:

$$\delta \int_{\mathcal{R}} H(q_1,p_1,\ldots,q_n,p_n)\, dq_1\, dp_1 \cdots dq_n\, dp_n = 0. \tag{2.12}$$

The quasiclassical optimization procedure is intuitively very clear: *find the region of fixed phase space volume within which the integral of the Hamiltonian is minimized.*

It is immediately evident that the unconstrained quasiclassical solution is ''exact,'' in the sense that the corresponding basis set satisfies Eq. (2.8). This is not generally true, however, if a constraint is imposed on $\hat{\rho}_N$—of separability, or otherwise. In all cases though, the solution must approach exactness in the large N limit. Moreover, we anticipate nearly optimal performance even for fairly small N, because it is $\mathrm{tr}(\hat{\rho}_N \hat{H})$ rather than $\hat{\rho}_N$ itself that is approximated. The latter varies much less than the former near the variational extremum, due to the locally quadratic form of the functional in this neighborhood.[37]

C. Quasiclassical estimate of efficiency

If the representational basis set $\hat{\rho}_N$ is constrained, then in general only some fraction of the $\hat{H}_{\rm pr}$ eigenvalues will be accurate. There is an excess of basis functions N over the number of accurate eigenvalues K. The ''efficiency'' of the constrained basis is defined as the ratio K/N. The quasiclassical phase space picture provides a good *a priori* estimate of this fraction. If $\mathcal{R}$ is the constrained region in question, then let $\mathcal{R}^{\rm un}$ be the largest unconstrained solution [$\hat{H}_0=\hat{H}$ in Eq. (2.10)] which is completely enclosed by $\mathcal{R}$. Qualitatively speaking, the areas of $\mathcal{R}$ lying outside of $\mathcal{R}^{\rm un}$ are effectively ''wasted,'' as they correspond to the $E>E_{\rm max}$ eigenstates that are only partially represented by $\hat{\rho}_N$. A quasiclassical estimate of the efficiency is thus given by the ratio of the phase space volume of $\mathcal{R}^{\rm un}$ to that of $\mathcal{R}$.

Our definition of quasiclassical efficiency is almost identical to that proposed previously by Fattal *et al.*,[33,34] but is more general, and obtained somewhat more rigorously. Their proposed optimal solution—based on a remapping scheme described many years earlier by Faist[38]—is essentially identical to the present result in the unconstrained 1D case. For more general situations however, for which there are constraints or multiple degrees of freedom, the phase space approach of Fattal *et al.* is incapable of providing the rigorously optimized result, because it does not establish the necessary quasiclassical correspondence for the basis set $\hat{\rho}_N$ itself.

The quasiclassical efficiency as defined above is also appropriate for DVR applications, because the transformation to the DVR basis—being a unitary transformation *within* the subspace $\hat{\rho}_N$—does not affect the eigenvalues of $\hat{H}_{\rm pr}$. For each degree of freedom q, the PSO DVR is constructed from the PSO basis set $|\phi_i\rangle$ in the standard way—i.e., by transforming to the eigenstates $|\varphi_i\rangle$ of the projected position operator $\hat{q}_{\rm pr}$, and using the eigenvalues of $\hat{q}_{\rm pr}$ as the DVR points.[6,8] By considering the quasiclassical analog of this procedure, incidentally, it is clear that the configuration space density $\rho^q(q)$ [Eq. (2.11)] can be roughly interpreted as the density of DVR points.

Using the ''wasted phase space'' picture described above, we can already apply a rudimentary phase space optimization to the standard 1D DVR calculations. In all such cases, the underlying basis set is somehow constrained—a sinc DVR, for instance, is constructed from the sinusoidal eigenfunctions of $\hat{p}^2$. Quasiclassically, the constrained $\mathcal{R}$ corresponding to the sinusoidal basis is the interior of a rectangle in the (q,p) phase space, centered along $p=0$. There are three parameters required to specify the rectangle, corresponding to the extent and spacing of the sinc DVR grid points. Roughly speaking, the optimal rectangle is the smallest one that contains $\mathcal{R}^{\rm un}$, as in Fig. 1(b), because this results in the smallest possible wasted area.

As a less trivial example, the Gauss–Hermite DVR is often employed,[8] because it is generally more efficient than a sinc DVR, and the analytic form for $T+V$ Hamiltonians is known. The reason is again clear from a phase space perspective. Here, we single out the smallest *ellipse*, rather than rectangle, that contains $\mathcal{R}^{\rm un}$. There are again three parameters specifying vertical and horizontal extents of the ellipse; but since $\mathcal{R}^{\rm un}$ is generally more oval-shaped than rectangular, the wasted area is reduced [Fig. 1(b)]. In practice, exact quantum optimization of the Gauss–Hermite DVR parameters is a difficult proposition;[8] instead, these values might be chosen to match the equilibrium point. If the energy range is large however, or the potential far from quadratic, then this choice will be considerably less efficient than the PSO choice presented here.

The simple 1D examples above are illuminating; but our primary focus is direct-product representations of many-dimensional Hamiltonians. This constraint is a rather severe one, in that it is equivalent to working with a collection of 1D regions $\mathcal{R}_k$—one for each degree of freedom k, residing on the ''marginal phase space'' (q_k,p_k). The individual $\mathcal{R}_k$'s are now completely unconstrained however, unlike the 1D examples just considered. This distinction is very evident in the rotationally invariant 2D example of Fig. 1. For any sinc DVR treatment, the complete region $\mathcal{R}=\mathcal{R}_x\times\mathcal{R}_y$ must be a four-dimensional box, in that $\mathcal{R}_x$ and $\mathcal{R}_y$ must each be rectangular. Because the potential has a narrow hole however, the shadow[39] of the unconstrained $\mathcal{R}^{\rm un}$ on to (q_x,p_k) [or (q_y,p_y)] is broad with a narrow spike, so that the smallest enclosing rectangle is much larger than the shadow region itself [Fig. 1(b)]. This can lead to great inefficiency, especially when compounded over several degrees of freedom.

Figure 1(a) demonstrates how the situation can be improved with a PSO DVR. The hole region is densely covered, but the representation of the remaining area is much more sparse, as desired. As a result, far fewer DVR points are required to perform the same calculation. On the other hand, the direct-product constraint is responsible for the ''crosslike'' pattern of points, which places extra points all along the rows and columns of the hole, resulting in some inefficiency. Nevertheless, the PSO DVR is far more efficient than a sinc DVR, which would extend the high density of the hole region throughout the entire space. Incidentally, the shadow regions are not quite the optimal solutions (Sec. III C); but they should nevertheless suffice for estimating the efficiency of the latter.

III. PHASE SPACE OPTIMIZATION OF DIRECT-PRODUCT BASES

In this section, the mathematical problem of optimizing the direct-product basis set (DPB) for representing a given Hamiltonian $\hat{H}$ is rigorously examined. We derive a stationarity condition for the exact quasiclassical solution, under the constraint of strong separability. We also present an iterative approximation scheme for practical use, and exhibit the explicit connection to optimal separable basis (OSB) theory. The latter is required in order to obtain the phase space optimized (PSO) marginal Hamiltonians.

A. Direct-product basis sets

Let $\hat{H}=H(\hat{q}_1,\hat{p}_1,\ldots,\hat{q}_n,\hat{p}_n)$ be an arbitrary nD Hamiltonian, not necessarily of the standard $T+V$ form. For

a given maximum energy of interest $E_{\max}$ and finite basis size N, we would like to specify the best possible DPB, with respect to the accuracy of the projected Hamiltonian eigenvalues below $E_{\max}$. The Hamiltonian is then represented in either the optimal basis itself, or in the DVR constructed from the latter (the direct-product PSO DVR). It is convenient to specify the DPB wave functions as the eigenfunctions of 1D marginal Hamiltonians $\hat{H}_k = H_k(\hat{q}_k, \hat{p}_k)$, where $(1 \leqslant k \leqslant n)$. We have

$$\Phi_{i_1 \cdots i_n}(q_1, \ldots, q_n) = \phi^1_{i_1}(q_1) \times \cdots \times \phi^n_{i_n}(q_n),$$
$$\hat{H}_k |\phi^k_{i_k}\rangle = \lambda^k_{i_k} |\phi^k_{i_k}\rangle, \tag{3.1}$$

where the i_k index the eigenstates of the $\hat{H}_k$.

The DPB wave functions of Eq. (3.1) are in principle infinite in number, and comprise a complete orthonormal basis of the underlying Hilbert space. In any computational application however, we are constrained to using finite basis sets only. It would clearly be desirable to use a direct energy truncation criterion, for which we discard all states $\Phi_{i_1 \cdots i_n}$ for which the expectation value of $\hat{H}$ is greater than some cutoff value $E_{\text{cut}} > E_{\max}$. This approach might be appropriate for a basis set representation (Sec. III D); however, for a DVR application, the set of basis functions is required to be ''rectangular.'' This means that *every* $\Phi_{i_1 \cdots i_n}$ for which $i_k \leqslant N_k$ for all k, must be included in the basis set. N_k is thus the number of one-dimensional functions associated with the kth degree of freedom, so that there are a total of $N = N_1 \times \cdots \times N_n$ DPB functions in all.

Despite the rectangularity constraint, an energy truncation of the basis set can still be utilized in a slightly less direct fashion. Assuming that the $\lambda^k_{i_k}$'s are arranged in increasing order, we simply choose the N_k's such that $\lambda^k_{N_k} \approx E_{\text{cut}}$, for each k. There are, however, many possible marginal Hamiltonians—with vastly different spectra—that have the same $\phi^k_{i_k}$ eigenstates. Consequently, the particular $\hat{H}_k$'s which are actually used must be related to $\hat{H}$ itself in some reasonable manner, if this energy truncation procedure is to be effective. We shall examine these issues more thoroughly in Sec. III B and in the Appendix. For now, we simply wish to emphasize the subtle, but important distinction between rectangularly constrained, and unconstrained, truncations of the basis set.

We now consider the UME density operator obtained from the rectangularly truncated basis set:

$$\hat{\rho}_N = \sum_{i_1=1}^{N_1} \cdots \sum_{i_n=1}^{N_n} |\Phi_{i_1 \cdots i_n}\rangle\langle\Phi_{i_1 \cdots i_n}| = \prod_{k=1}^{n} \hat{\rho}_k. \tag{3.2}$$

The resultant density operator $\hat{\rho}_N$ is a separable product of 1D density operators, $\hat{\rho}_k$. Moreover, each of the $\hat{\rho}_k$'s is also a UME, albeit one that involves the kth degree of freedom only. These facts are evident from Eqs. (3.1) and (3.2), from which we find

$$\hat{\rho}_k = \sum_{i_k=1}^{N_k} |\phi^k_{i_k}\rangle\langle\phi^k_{i_k}|. \tag{3.3}$$

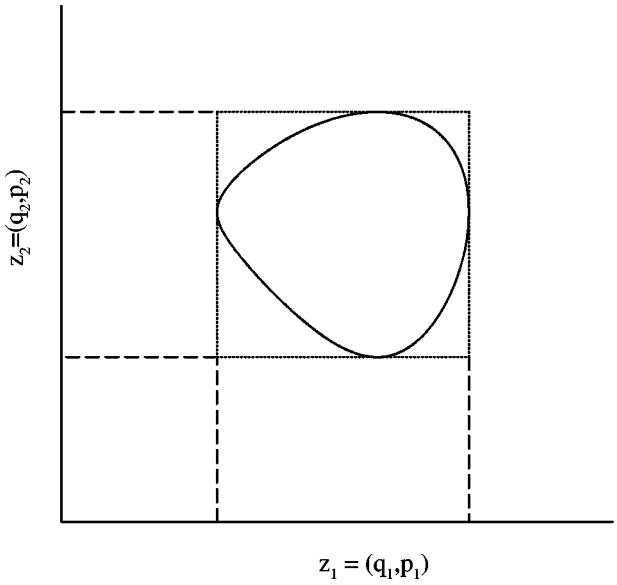

FIG. 2. Schematic of four-dimensional phase space of a 2D Hamiltonian, with each axis representing a single degree of freedom. Solid curve represents the contour $H(q_1,p_1,q_2,p_2) = E^{(0)}_{\max}$, as well as the limits of the unconstrained phase space region $\mathcal{R}^{\text{un}}$. Constrained regions $\mathcal{R}$ correspond to rectangles, with the dotted-line choice above being the zeroth-order optimum. Shadows cast on the marginal phase spaces ($\mathcal{R}^{(0)}_1$ and $\mathcal{R}^{(0)}_2$) are the same for both $\mathcal{R}$ and $\mathcal{R}^{\text{un}}$.

For the present purpose, Eqs. (3.2) and (3.3) constitute the correct constraint on the variational minimization of Eq. (2.8).

As discussed in Sec. II B, a reasonable approximation of the minimum of Eq. (2.9) is obtained by replacing $\hat{\rho}_N$ with the quasiclassical Thomas–Fermi distribution on phase space. Thus, for the present direct-product application, we must determine the quasiclassical constraint analogous to Eqs. (3.2) and (3.3). This is very straightforward however; the separable direct-product constraint implies a quasiclassical density of the form

$$\rho(q_1,p_1, \ldots, q_n,p_n) = \rho_1(q_1,p_1) \times \cdots \times \rho_n(q_n,p_n), \tag{3.4}$$

where each of the $\rho_k(q_k,p_k)$'s is itself a uniform distribution over a region $\mathcal{R}_k$ in the kth marginal phase space. The product distribution $\rho(q_1,p_1,\ldots,q_n,p_n)$ extends over a $2n$-dimensional region $\mathcal{R}$, which is ''rectangular'' (actually cylindrical) with respect to the individual marginal phase spaces of the n degrees of freedom (Fig. 2). *Within* each marginal phase space however, the $\mathcal{R}_k$ may describe any arbitrary shape (Fig. 3).

B. Phase space optimization

To optimize the direct product representation in accord with Eq. (2.12), we must vary the individual shadow regions $\mathcal{R}_k$ until the integral of the Hamiltonian $H(q_1,p_1,\ldots,q_n,p_n)$ within the product region $\mathcal{R}$ is minimized (Fig. 3). The total phase space volume $\mathcal{V}$ enclosed by $\mathcal{R}$ must remain fixed throughout the variation, implying a constant basis size $N \approx \mathcal{V}/(2\pi)^n$. Note, however, that the individual marginal areas $\mathcal{A}_k$ (enclosed by the two-dimensional regions $\mathcal{R}_k$) are

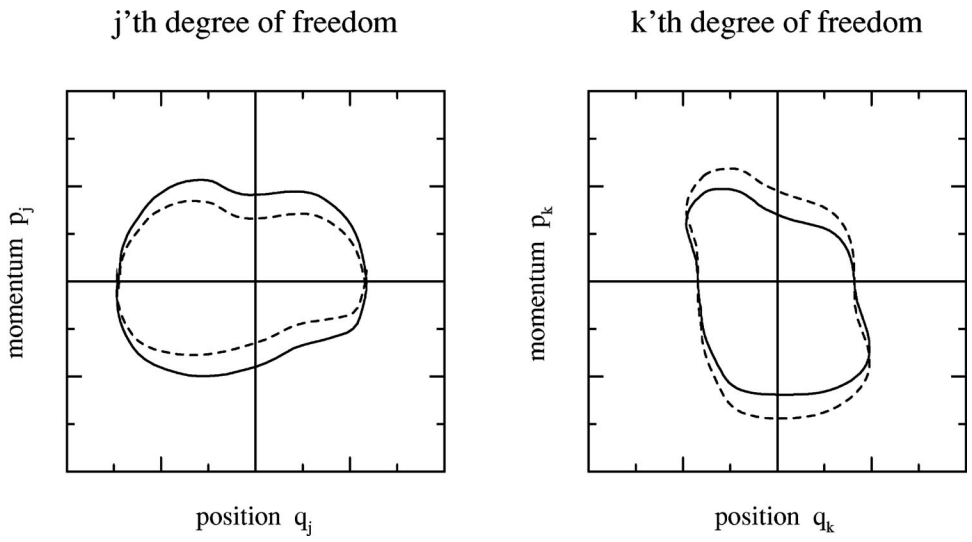

FIG. 3. Two marginal phase spaces for a non-$T+V$ Hamiltonian of arbitrary dimensionality. Solid curves enclose the marginal regions $\mathcal{R}_k$, etc., whose product over all degrees of freedom defines $\mathcal{R}$. In optimizing the latter, the $\mathcal{R}_k$ may be varied arbitrarily, as indicated schematically by the dashed curves above. However, the variation must not alter the total volume $\mathcal{V}$, i.e., the product of the areas $\mathcal{A}_k$ enclosed by each of the marginal regions.

not constrained by the variation—apart from the overall condition that $\mathcal{V}=\mathcal{A}_1\times\cdots\times\mathcal{A}_n$. This implies that the N_k need not be specified *a priori*, but are determined automatically by the optimization itself.

Mathematically, the procedure described above is a very straightforward application of the standard variational calculus.[37] Each two-dimensional marginal region $\mathcal{R}_k$ is uniquely represented by a multivalued function $p_k^{\text{ext}}(q_k)$, specifying the boundary of the region. The minimization is a constrained optimization with respect to variations of the $p_k^{\text{ext}}(q_k)$. In the Appendix, we derive the stationarity condition for the optimal solution, as well as a simple interpretation of the $p_k^{\text{ext}}(q_k)$. These results are best understood in terms of OSB theory.

An OSB description is also motivated by the following concern. Suppose that the quasiclassical optimum $\rho(q_1,p_1,\ldots,q_n,p_n)$ is obtained for a given system. On the surface of it, the problem is solved, because each $\rho_k(q_k,p_k)$ specifies a basis set subspace for the kth degree of freedom. However, an explicit association between $\rho_k(q_k,p_k)$ and $\hat{\rho}_k$ is still required in order to obtain the actual basis. This is not accomplished directly, but through the Wigner–Weyl correspondence of the associated marginal Hamiltonians $\hat{H}_k$ (Sec. II). It is therefore necessary to obtain explicit classical expressions $H_k(q_k,p_k)$ for the marginal Hamiltonians.

Since ''closeness'' to the true Hamiltonian is a necessary criterion in this regard (Sec. III A), the OSB marginal Hamiltonians are a natural choice; but these must be modified somewhat for the projected, quasiclassical situation at hand. Given that the Eq. (2.4) result for $\hat{H}_x$ can be interpreted as the *average* of $\hat{H}$ with respect to y (apart from a constant), it is natural to use an analogous formula here. We therefore take $H_k(q_k,p_k)$ (apart from a constant) to be the integral of $\rho(q_1,p_1,\ldots,q_n,p_n)H(q_1,p_1,\ldots,q_n,p_n)$ divided by the integral of $\rho(q_1,p_1,\ldots,q_n,p_n)$, with respect to all phase space coordinates except q_k and p_k. The correspondence with the trace relations of Eqs. (2.2) and (2.5) is evident from Eq. (2.9).

Having specified the marginal $H_k(q_k,p_k)$'s, the corresponding operators $\hat{H}_k$ are obtained using the Wigner–Weyl rule. It is then a straightforward matter to specify the associated UME $\hat{\rho}_k$'s as the lowest $N_k\approx\mathcal{A}_k/(2\pi)$ eigenstates of the $\hat{H}_k$'s. There is a possible difficulty to this procedure, however. Implicitly, we made use of the optimal $\rho_k(q_k,p_k)$'s to obtain the $H_k(q_k,p_k)$'s, via strongly separable OSB theory. In turn, the contours of the $H_k(q_k,p_k)$ functions give rise to regions $\mathcal{R}_k$ which are the ones ultimately associated with the quantum UMEs—but these may or may not be the same $\mathcal{R}_k$'s that we started with! Intuitively, we would like the two sets of $\mathcal{R}_k$'s to be the same, of course. Whereas in the general case they must be distinct, it turns out that their equivalence is *precisely* the stationarity condition heralding the quasiclassical optimum (Appendix).

In other words, the stationary solution of Eq. (2.12) satisfies the following self-consistency relation, with respect to the strongly separable OSB marginal Hamiltonians:

$$H_k(q_k,p_k)=\frac{\mathcal{A}_k}{\mathcal{V}}\int H(q_1,p_1,\ldots,q_n,p_n)\times\prod_{j\neq k}\rho_j(q_j,p_j)\,dq_j\,dp_j-E_0,\qquad(3.5)$$

$$\rho_j(q_j,p_j)=\Theta(E_{\max}-H_j(q_j,p_j)).$$

In Eq. (3.5), the area $\mathcal{A}_k$ is $\int\rho_k(q_k,p_k)\,dq_k\,dp_k$, and the constant

$$E_0=\left(\frac{n-1}{n}\right)\langle H\rangle,$$
$$\langle H\rangle=\frac{\int_{\mathcal{R}}H(q_1,p_1,\ldots,q_n,p_n)\,dq_1\,dp_1\cdots dq_n\,dp_n}{\int_{\mathcal{R}}dq_1\,dp_1\cdots dq_n\,dp_n}\qquad(3.6)$$

is analogous to the $\langle V\rangle$ terms in Eq. (2.5).

Note that the $\mathcal{R}_k$-defining maximum energy contours $H_k(q_k,p_k^{\rm ext}(q_k))=E_{\rm max}$ are all characterized by the same value of $E_{\rm max}$, for each of the n degrees of freedom; the value itself is arbitrary, however (Appendix). With the E_0 term included as above, it is reasonable to interpret $E_{\rm max}$ as the maximum energy of interest, in accord with Sec. III A. Note, however, that it is not the energy $E_{\rm max}$, but the total phase space volume $\mathcal{V}$, which is fixed in the variation; consequently, the value of $E_{\rm max}$ is not determined until after the variation is completed.

It turns out that in a purely quantum treatment, a similar relationship to Eq. (3.5) also holds, i.e., the OSB result gives rise to marginal Hamiltonians $\hat{H}_k$ whose eigenstates are consistent with those obtained by minimizing $\mathrm{tr}(\hat{\rho}_N\hat{H})$. The analogy between quantum and quasiclassical optimizations is evidently very tight; though the end results are not necessarily identical (Sec. II B). In any event, it should be emphasized that in neither case is the OSB relation imposed *a priori*; Eq. (2.8) or (2.12) alone is thus sufficient for determining both the basis set *and* the marginal Hamiltonians.

It is worth discussing the special case of $T+V$ Hamiltonians briefly. The optimal $H_k(q_k,p_k)$'s are not presumed *a priori* to be of this simple and convenient form, since the range of marginal Hamiltonians is completely unconstrained in the variational optimization. Nevertheless, it can be shown from Eq. (3.5) that the marginal Hamiltonians are indeed of the kinetic-plus potential variety. In other words,

$$H_k(q_k,p_k)=\frac{p_k^2}{2m_k}+V_k(q_k). \tag{3.7}$$

Consequently, the problem of finding the optimal $H_k(q_k,p_k)$'s reduces to that of finding the optimal marginal potential functions, $V_k(q_k)$. This situation is clearly desirable from a computational perspective, because the 1D $T+V$ Hamiltonians are easy to deal with numerically, and also because the optimization procedure itself now involves only the n-dimensional configuration space, rather than the entire $2n$-dimensional phase space.

The self-consistency relations of Eq. (3.5) can be rewritten directly in terms of the marginal potentials, as follows:

$$\begin{aligned} V_k(q_k)&=(2\pi)^{n-1}\frac{\mathcal{A}_k}{\mathcal{V}}\int V(q_1,\ldots,q_n)\\ &\quad\times\prod_{j\neq k}\rho_j^q(q_j)\,dq_j-E_0^k,\\ \rho_j^q(q_j)&=(2\pi)^{-1}\int \rho_j(q_j,p_j)\,dp_j\\ &=\pi^{-1}\,\Theta(E_{\rm max}-V_j(q_j))\sqrt{2m_k[E_{\rm max}-V_j(q_j)]}. \end{aligned} \tag{3.8}$$

The constant term is

$$E_0^k=\left(\frac{n-1}{n}\right)\langle H\rangle-\sum_{j\neq k}\frac{\langle p_j^2\rangle}{2m_j}, \tag{3.9}$$

where the expectation values are as in Eq. (3.6). Note that the E_0^k are now formally dependent on k, in contrast to Eq. (2.5). The reason for this discrepancy is subtle, but ultimately reflects the finite constraint present in the Eq. (3.8) case. In practice, the k dependence of the E_0^k's is often slight, in which case they can be replaced with E_0, or with $[(n-1)/n]\langle V\rangle$.

C. Obtaining the marginal Hamiltonians

Equations (3.5) and (3.8) represent conditions of stationarity only, and do not in and of themselves provide a recipe for obtaining a solution. These equations are very similar to the self-consistent field equations of the Hartree theory,[40–42] in quite a number of respects. Indeed, Hartree theory suggests a natural procedure for actually obtaining solutions here—namely, to select a zeroth-order approximation $H_k^{(0)}$ and $\rho_k^{(0)}$, and then to obtain successively more accurate approximations via iteration, until self-consistency is achieved to sufficient accuracy.

The determination of $\rho_k^{(l)}$ from the contours of $H_k^{(l)}$ is trivial; whereas going from $\rho_k^{(l)}$ to $H_k^{(l+1)}$ requires evaluating the n integrals of the first line of Eq. (3.5) or (3.8). Numerically, these integrations are fairly straightforward, and would tend to make good candidates for a Monte Carlo calculation.[43] Less computational effort is required than for overlap integrals, for instance, because the integrands required here are generally smooth. Nevertheless, if n is quite large, the numerical integrations might be CPU intensive if many iterations are required.

For practical applications, it is not necessary to converge to very high accuracy; getting anywhere near the quasiclassical optimum should yield an extremely efficient quantum basis set. Moreover, there is a natural zeroth-order approximation—to be described shortly—which is fairly accurate on its own, and easily obtained. Starting with this approximation, we anticipate that only a few iterations should be required to obtain an accuracy reasonable for most purposes. This is borne out by the examples considered in Secs. IV and V, where only one iteration is applied. In the case of Sec. IV, this is nevertheless sufficient to achieve full convergence.

The zeroth-order approximation referred to in the previous paragraph is obtained by simply projecting the *unconstrained* quasiclassical solution on to each of the marginal phase spaces—as was already considered in Sec. II C. If $E_{\rm max}^{(0)}$ is the zeroth-order $E_{\rm max}$, then the optimal unconstrained $\rho(q_1,p_1,\ldots,q_n,p_n)$ is given by

$$\begin{aligned} &\rho^{\rm un}(q_1,p_1,\ldots,q_n,p_n)\\ &\quad\equiv\Theta(E_{\rm max}^{(0)}-H(q_1,p_1,\ldots,q_n,p_n)) \end{aligned} \tag{3.10}$$

(Section II B). By varying the $\{q_{j\neq k},p_{j\neq k}\}$ coordinates arbitrarily in Eq. (3.10) above, we obtain the allowed range of (q_k,p_k) values, and hence the shadow of $\rho^{\rm un}(q_1,p_1,\ldots,q_n,p_n)$ on to the kth marginal phase space. The product of all n such regions $\mathcal{R}_k^{(0)}$ is the zeroth-order constrained $\mathcal{R}^{(0)}$.

This definition of $\mathcal{R}^{(0)}$ is a very natural choice, in that it is the smallest possible product region containing $\mathcal{R}^{\rm un}$ that can be constructed (Fig. 2). The rectangularity constraint of the former, however, implies that the volume of $\mathcal{R}^{(0)}$ is

larger than that of $\mathcal{R}^{\rm un}$. We can expect the PSO DVR efficiency (Sec. II C) to decrease as the dimensionality is increased, and also as the potential function becomes increasingly nonseparable. Note that even for a strongly separable system, the quasiclassical efficiency estimate must be less than unity—even though the resultant eigenvalues are all exact. This is because the basis set truncation is rectangularly constrained, rather than unconstrained. Consequently, the $\rho^{(0)}$ distribution itself is not the optimal one; but it should generally serve as a good zeroth-order approximation.

The corresponding $H_k^{(0)}(q_k,p_k)$ functions, incidentally, are obtained in the following way: with (q_k,p_k) fixed, vary the $\{q_{j\neq k},p_{j\neq k}\}$ arbitrarily within the range of Eq. (3.10), and set the *minimum* value of $H(q_1,p_1,\ldots,q_n,p_n)$ as the value for $H_k^{(0)}(q_k,p_k)$. For $T+V$ Hamiltonians, this reduces to a minimization of the potential only, with respect to all but one of the n configuration space coordinates. This procedure has been successfully applied in previous applications.[15,35] Note that the numerical effort involved in obtaining $H_k^{(0)}$ is comparable to that of the more accurate $H_k^{(1)}$, which requires just a single application of Eq. (3.5) or (3.8). We therefore advocate the use of the latter.

D. Constructing the PSO DVR

Having defined the optimal marginal Hamiltonian operators $\hat{H}_k$, we now turn to the construction of the PSO DVR itself. The first step is to decide how many basis functions will be used to represent each degree of freedom. We observe that the quasiclassical self-consistency relations of Sec. III C give rise to a rectangular truncation criterion that is exactly analogous to that of Sec. III A. In the quasiclassical case, it is $E_{\rm max}$ itself that is used in the truncation. Were we to translate this ''verbatim'' into quantum mechanics (by setting $E_{\rm cut}=E_{\rm max}$), then we would be allowing the quasiclassical procedure to determine both $E_{\rm max}$ and N. In practice however, it is much better to decouple these two parameters, and to use a basis size that is larger than the quasiclassical value, by setting $E_{\rm cut}>E_{\rm max}$ (Sec. III A). This means that the total basis size N can be varied *independently* of the number of desired accurate eigenvalues K in a highly efficient manner—a very desirable feature that has been lacking from most previous DVR implementations.

We have thus far ignored the fact that a DVR is not quite a true representation, because the ''residual'' $\hat{\Delta}=\hat{H}-\hat{H}_0$ is represented only *approximately*. The ''quadrature error'' introduced by the DVR approximation is fundamentally distinct from the representational error discussed heretofore, and only the former is accounted for in the optimization of Eq. (2.8). Nevertheless, it is unlikely that the results would be affected much if quadrature were incorporated—at least for the $T+V$ Hamiltonians, for which $\hat{\Delta}=\hat{V}-\hat{V}_1\cdots-\hat{V}_n$ has a potential-like form. Quadrature error decreases rapidly as the basis size is increased, and is further reduced by decreasing the magnitude—and increasing the smoothness—of the residual potential. In the PSO DVR case, the marginal potentials are smoother than $V(q_1,\ldots,q_n)$, so it is the latter that generally determines the smoothness of $\Delta(q_1,\ldots,q_n)$. But this contribution is the same, regardless of which marginal potentials are chosen; thus, smoothness is not expected to play a significant role in the optimization procedure.

In contrast, the overall size of the residual potential does vary quite a bit with the choice of the marginal potentials. By its very definition however, the OSB approximation is precisely the one which minimizes the size of the residual.[4] Thus, in addition to (nearly) optimizing the representation, the quasiclassical procedure also minimizes the primary contribution to quadrature error. This fortuitous situation is obviously quite relevant for DVR applications—although it should be mentioned that a rigorous characterization of quadrature errors is still lacking for the general PO DVR case. Nevertheless, it is expected that the quasiclassical optimization method presented herein may offer a significant improvement for both basis set and DVR calculations. Examples of both are considered in the next two sections.

IV. COUPLED HARMONIC OSCILLATOR EXAMPLE

We start with the trivial uncoupled harmonic oscillator system,

$$\hat{H}=\frac{\hat{p}_x^2}{2}+\frac{\hat{p}_y^2}{2}+\frac{\hat{x}^2}{2}+\frac{\hat{y}^2}{2}. \tag{4.1}$$

Since the Hamiltonian is already strongly separable to begin with, it is obvious that the best quantum-mechanical marginal Hamiltonians must be $\hat{H}_x=(\hat{p}_x^2+\hat{x}^2)/2$ and $\hat{H}_y=(\hat{p}_y^2+\hat{y}^2)/2$. It is nevertheless instructive to verify that the quasiclassical method also returns this result.

The unconstrained region $\mathcal{R}^{\rm un}(x,p_x,y,p_y)$ is the interior of a hypersphere, whose shadows on the x and y marginal phase spaces are circular disks. Taking these regions as our zeroth-order $\mathcal{R}_x^{(0)}$ and $\mathcal{R}_y^{(0)}$, we find that they correspond to zeroth-order marginal Hamiltonians $H_x^{(0)}(x,p_x)=(p_x^2+x^2)/2$, etc. It is easy to show however, that the first-order results $H_x^{(1)}$, etc., are identical to the zeroth-order ones. These approximations are therefore self-consistent to begin with, and thus equivalent to the quasiclassical optimum. Moreover, the quasiclassical solution is seen to correspond exactly to the quantum solution. Similar comments would hold for any strongly separable system.

The coupled oscillator system

$$\hat{H}=\frac{\hat{p}_x^2}{2}+\frac{\hat{p}_y^2}{2}+\frac{\hat{x}^2}{2}+\frac{\hat{y}^2}{2}-\epsilon\,\hat{x}\hat{y} \tag{4.2}$$

is a bit more interesting. In reality, the above Hamiltonian decouples in a different set of coordinates, so that the eigenvalue spectrum can be obtained analytically. Specifically, if the coordinates (x,y) are rotated by 45°, then $\hat{H}$ becomes the sum of two harmonic oscillators with different frequencies [Fig. 4(a)]. The eigenvalues are given in terms of the two (non-negative) quantum numbers m and n as

$$E_{mn}=\frac{(m+1/2)}{\sqrt{1-\epsilon}}+\frac{(n+1/2)}{\sqrt{1+\epsilon}}, \tag{4.3}$$

where $0\leqslant\epsilon<1$ is a measure of the difference between the two fundamental frequencies.

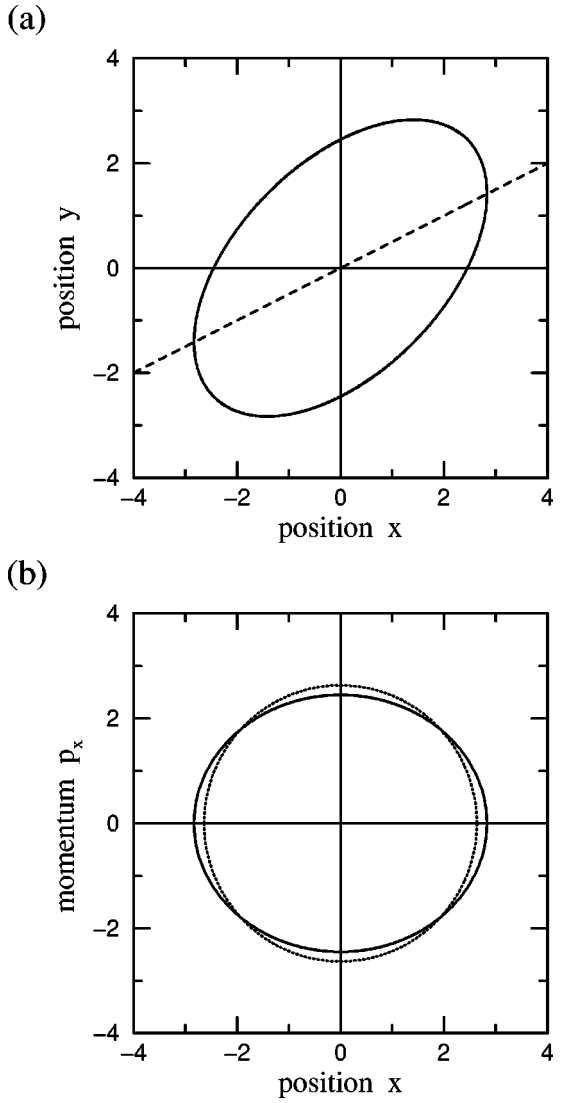

FIG. 4. Shadows of unconstrained region $H(x,p_x,y,p_y)\leqslant 3.0$ on to relevant subspaces, for coupled oscillator system $H=(p_x^2+p_y^2)/2+(x^2+y^2-xy)/2$. Region boundaries are indicated by solid curves. (a) Configuration space, displaying $x-y$ correlation which decouples under a 45° rotation. Dashed line is location of the $V(x,y)$ minimum for each x. (b) Marginal x phase space (identical to y). The result is flattened slightly in comparison with the true optimum, indicated by the dotted curve.

Because of symmetry, the marginal solutions for the x and y degrees of freedom must be identical. From the form of Eq. (4.2), we anticipate that $H_x(x,p_x)=(p_x^2+x^2)/2$,etc.; but this should be verified via explicit calculation. We begin with the zeroth-order marginal Hamiltonians. These are easily found to be $H_x^{(0)}(x,p_x)=[p_x^2+(1-\epsilon^2)x^2]/2$, etc. Note that the marginal potential is somewhat shallower than expected, to an extent depending on ϵ. This results in zeroth-order shadow regions $\mathcal{R}_x^{(0)}$, etc., which are oblong ellipses, rather than circular discs [Fig. 4(b)].

Integrating $H(x,p_x,y,p_y)$ over the product region $\mathcal{R}^{(0)}$ using Eq. (3.8), we find the first-order results to be in keeping with our intuitive expectations:

$$H_x^{(1)}(x,p_x)=(p_x^2+x^2)/2,$$
$$H_y^{(1)}(y,p_y)=(p_y^2+y^2)/2. \tag{4.4}$$

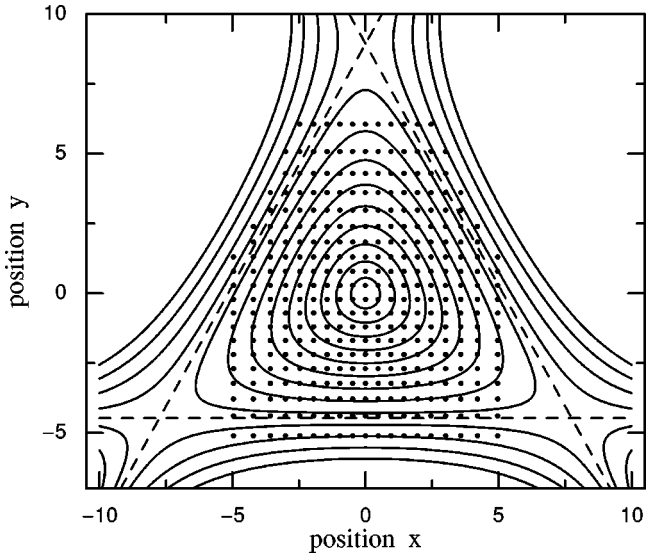

FIG. 5. Contour plot of 2D Henon–Heiles potential $V(x,y)=x^2/2+y^2/2+(x^2y-y^3/3)/\sqrt{80}$, exhibiting C_{3v} symmetry. Dashed lines indicate the dissociation triangle at $V(x,y)=E_{\rm dis}=13.33\overline{3}$. Solid circles represent the PSO DVR grid truncated via $V(x,y)<V_{\rm cut}=18.0$, for the basis truncation energy $E_{\rm cut}=18.0$.

Continuing the process, $\mathcal{R}_x^{(1)}$ and $\mathcal{R}_y^{(1)}$ are clearly circular disks, and thus distinct from $\mathcal{R}_x^{(0)}$, etc.

However, the second-order marginal Hamiltonians are once again $H_x^{(2)}(x,p_x)=(p_x^2+x^2)/2$, etc. We have therefore converged to the exact quasiclassical solution after just a *single* iteration. Moreover, it is easily shown that the corresponding quantum operators are also equivalent to the optimal ones. It should be noted that the present example is somewhat special, in that the optimal solution does *not* depend on the maximum energy $E_{\rm max}$. This can be traced to the odd-symmetric form of the interaction potential, which effectively vanishes in all of the Eq. (3.8) integrations.

Since the optimal strongly separable approximation to $\hat{H}$ is just the uncoupled harmonic oscillator of Eq. (4.1), there is not much to be gained from a full DVR calculation for this model system. We will, however, consider the accuracy that can be obtained by the PSO DPB representation itself, in the limit that $\epsilon\rightarrow 0$. In this limit, Eq. (4.3) becomes

$$E_{mn}\approx(m+n+1)+\epsilon\frac{(n-m)}{2}, \tag{4.5}$$

whereas the strongly separable result is equal to just the first parenthetical expression above. Assuming the range of n and m values to be identical, we find the strongly separable error to be positive as often as it is negative. We have, of course, neglected to include the residual term $\Delta(x,y)=-\epsilon xy$ in our finite representation. The inclusion of this term would necessarily result in approximate eigenvalues that are all too large; consequently, the representational errors in the PSO DPB must be zero, to second order in ϵ.

V. TWO-DIMENSIONAL HENON–HEILES EXAMPLE

A. Henon–Heiles potential

In this section, we apply the PSO DVR method to the anharmonic Henon–Heiles system. This simple, but nontrivial, 2D model system has long been used as a benchmark for numerical methods.[44–49] Analytically, it is equivalent to the uncoupled harmonic oscillator of Eq. (4.1), plus an additional interaction potential,

$$V_{\rm int}(\hat{x},\hat{y}) = \lambda\left(\hat{x}^2\hat{y} - \frac{\hat{y}^3}{3}\right). \tag{5.1}$$

A naive separable approximation would simply ignore the contribution of Eq. (5.1). This would be accurate at low energies, if λ were sufficiently small. At higher energies however, the classical system becomes chaotic for the value of λ used in this paper and elsewhere[44–48] ($\lambda = 1/\sqrt{80}$). In this case, Eq. (4.1) is no longer an adequate separable approximation.

For the value of λ specified, the Henon–Heiles system has a ''dissociation'' threshold at $V(x,y) = E_{\rm dis} = 13.33\overline{3}$, where $V(x,y)$ is the full potential (Fig. 5). This particular contour is an equilateral triangle centered at the origin. In general, the potential possesses threefold symmetry, and decreases to negative infinity as one extends beyond the dissociation triangle in the direction of the triangular corners (saddle points). Quantum mechanically, this implies that there are no true bound states, only quasibound resonances. For the states within the energy range considered in this paper however ($K = 36$ desired eigenvalues), there is very little tunneling—no more than about one part in 10^{10} or so. For the most part, this is insignificant in comparison to the accuracies obtained in our eigenvalue calculations, and can be ignored. The negative divergence of the potential will play an important role in the determination of the optimal marginal potentials, however.

Figure 5 is a contour plot of the Henon–Heiles potential for the λ value specified. The C_{3v} symmetry induced by the interaction potential is very evident in all but the lowest energy bound state contours. It also gives rise quantum mechanically to a degenerate eigenvalue structure. In previous quantum calculations, other authors[45,47] have made use of coordinates that exploit this symmetry. We deliberately avoid doing so, and stick to a conventional Cartesian coordinate treatment, in order to test the efficiency of the PSO DVR method for a coordinate representation that is substantially nonseparable.

B. Marginal Hamiltonians

Using the iterative approximation method of Sec. III C, we shall determine the zeroth-order and first-order marginal Hamiltonians in x and y, for a variety of $E^{(0)}_{\rm max}$ values below the dissociation threshold, $E_{\rm dis}$. Formally, the unconstrained regions $\mathcal{R}^{\rm un}$ are *not* simply connected—consisting of a finite piece within the dissociation triangle (Fig. 5), and three disconnected pieces lying outside of the triangle and extending to infinity. This reflects the fact that the true eigenfunctions are actually resonances, rather than bound states. In keeping with our bound state approximation however, we discard the external regions, and consider only the portion of $\mathcal{R}^{\rm un}$ which lies within the dissociation triangle. The constrained region $\mathcal{R}$ does extend beyond these boundaries, however.

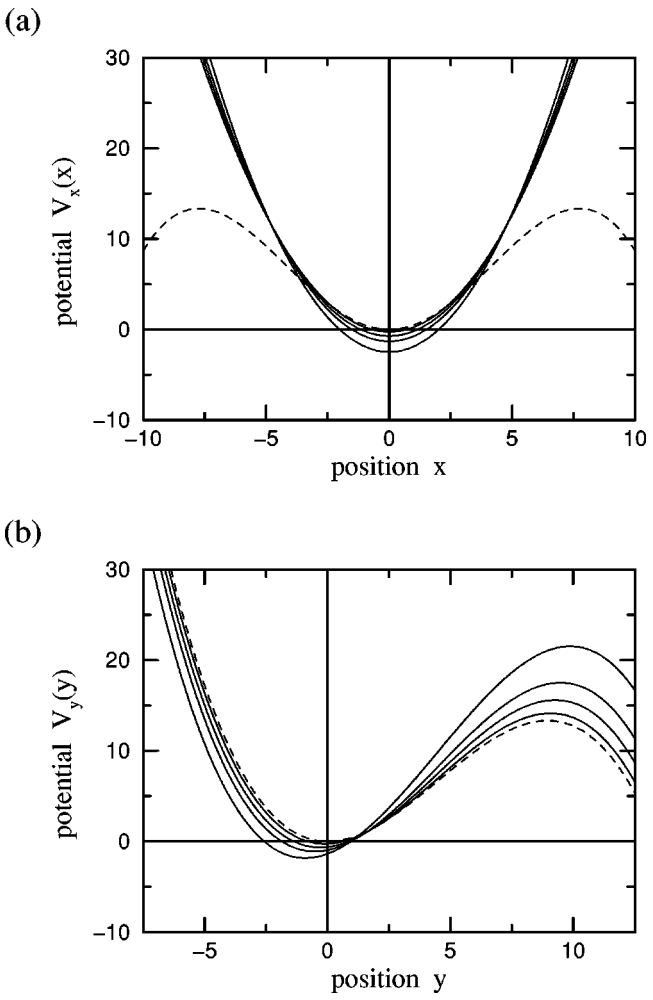

FIG. 6. Marginal potentials for 2D Henon–Heiles system: zeroth order (dashed), and first order (solid). The latter are presented for various maximum energies $E^{(0)}_{\rm max} = \{2.0, 5.0, 8.0, 12.0\}$, where higher energies are identified with lower potential values near the origin. (a) Marginal x potentials, $V_x(x)$; first-order curves are quadratics. (b) Marginal y potentials, $V_y(y)$; first-order curves are cubics, where the barrier height increases with $E^{(0)}_{\rm max}$.

The zeroth-order, or minimal potentials, can be obtained analytically, and are found to be

$$V^{(0)}_x(x) = x^2 + \frac{1-(4\lambda^2 x^2+1)^{3/2}}{12\lambda^2},$$
$$V^{(0)}_y(y) = \frac{y^2}{2} - \frac{\lambda y^3}{3}. \tag{5.2}$$

Equation (5.2) holds for all values of $E^{(0)}_{\rm max}$. The $V^{(0)}_y(y)$ potential has a local minimum at the origin, but reaches a maximum value of $E_{\rm dis}$ at $y = 4\sqrt{5} \approx 8.944$, beyond which it drops to negative infinity. This is not surprising given the nature of $V(x,y)$; moreover a separation of $\mathcal{R}^{(0)}_y$ into bounded and unbounded portions exists only when the energy is less than $E_{\rm dis}$. Perhaps more surprising is the behav-

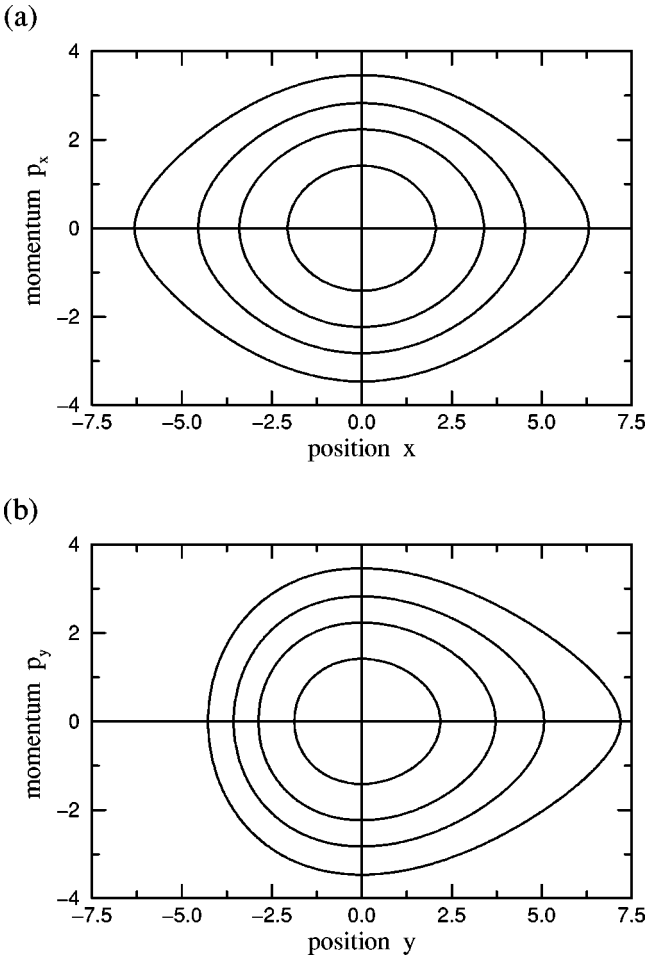

FIG. 7. Marginal phase space regions for 2D Henon–Heiles system: (a) x phase space region $\mathcal{R}_x$; (b) y phase space region $\mathcal{R}_y$. Zeroth-order boundaries are presented for various maximum energies $E_{\max}^{(0)}=\{2.0,5.0,8.0,12.0\}$, where higher energies are identified with larger enclosed areas. With the vertical axis interpreted as $\pi\times$ probability, the $p>0$ curves also represent the density of DVR points along x or y.

ior of the even $V_x^{(0)}(x)$ potential, which drops to negative infinity in *both* directions, after attaining a maximum value of $E_{\rm dis}$ at $|x|=2\sqrt{15}\approx 7.746$ (Fig. 6).

If only the bounded portions of $\mathcal{R}_x^{(0)}$ and $\mathcal{R}_y^{(0)}$ are retained, then the constrained density $\rho^{(0)}(x,y)$ is well-defined only when $E_{\max}^{(0)}<E_{\rm dis}$. Quasiclassically, this does not pose a major problem; however, the corresponding zeroth-order quantum treatment would be severely restricted, in that the truncation energy $E_{\rm cut}$ would also have to be less than $E_{\rm dis}$, in order to restrict the basis to quasibound states. The accuracy of such a representation would therefore diminish rapidly as the dissociation threshold was approached. In any event, the zeroth-order quasiclassical density functions $\rho_x^0(x)$ and $\rho_y^0(y)$ are presented in Fig. 7 for several different $E_{\max}^{(0)}$ values.

By substituting the zeroth-order density functions into the first line of Eq. (3.8), we obtain the first-order marginal potentials, $V_x(x)=V_x^{(1)}(x)$ and $V_y(y)=V_y^{(1)}(y)$ (for convenience, we omit first-order superscripts in the subsequent discussion). These turn out to be simple polynomial expressions, and in that sense are more straightforward than the minimal potentials. However, there is now an energy dependence which manifests itself in the polynomial constants. These cannot be determined analytically, but must be calculated separately for each $E_{\max}^{(0)}$ value of interest. Being only one-dimensional however, the corresponding integrals are numerically trivial.

Although we have calculated the polynomial constants numerically for all $E_{\max}^{(0)}$ values considered in this paper, we have also derived a general analytical approximation, valid in the small λ limit:

$$V_x(x)\approx\frac{x^2}{2}+\frac{E_{\max}^{(0)}}{4}-E_0,$$
$$V_y(y)\approx\frac{y^2}{2}+\frac{E_{\max}^{(0)}}{4}-\lambda\left(\frac{y^3}{3}-\frac{E_{\max}^{(0)}y}{4}\right)-E_0, \tag{5.3}$$

where E_0 is substituted for E_0^k (Sec. III B). For the $\lambda=1/\sqrt{80}\approx 0.1118$ value used in this paper, the relative errors of the Eq. (5.3) approximate potentials are no larger than a few percent, over the relevant coordinate ranges. Moreover, the quadratic and cubic terms of the $V_y(y)$ expression are exact. We have used the numerically integrated constants in all of the computational work presented in Secs. V C and V D, and also for the marginal potential plots of Fig. 6. Nevertheless, Eq. (5.3) is pedagogically useful.

We observe, for instance, that $H_x(x,p_x)$ is now a simple harmonic oscillator. The standard Gauss–Hermite DVR is therefore optimal for this coordinate, to first order. Moreover, the negative divergence associated with $V_x^{(0)}(x)$ is no longer present, so that the basis size N_x is completely unrestricted. According to Eq. (5.3), the marginal $V_x(x)$ potential is energy independent, apart from the constant term. In reality however, there is a slight narrowing of the harmonic well with increasing $E_{\max}$, as is clear from Fig. 6.

The $V_y(y)$ potential function is a cubic expression, which therefore retains the negatively divergent behavior in the large y limit. This implies an upper limit on $E_{\rm cut}$, and on the basis size N_y. Nevertheless, the situation is much improved over the zeroth-order case, in that the barrier height increases substantially with increasing $E_{\max}^{(0)}$ (Fig. 6), owing to the energy dependence of the linear term of Eq. (5.3). Consequently, even if $E_{\max}^{(0)}\approx E_{\rm dis}$, the resultant $V_y(y)$ well is deep enough to sustain quite a number of quasibound basis functions with energies above $E_{\rm dis}$.

C. Direct-product basis

The first-order marginal potentials $V_x(x)$ and $V_y(y)$, as determined in Sec. V B, have been optimized for a variety of different $E_{\max}^{(0)}$ values. For the remainder of this section, we consider only the specific case $E_{\max}^{(0)}=12.0$, for which the first-order marginal potentials are given explicitly as

$$V_x(x)=0.6106\,x^2-2.4923,$$
$$V_y(y)=\frac{y^3}{3\sqrt{80}}+\frac{y^2}{2}+1.0143\,y-1.3441. \tag{5.4}$$

The $V_y(y)$ potential attains a maximum value of 21.543 at $y=y_0\approx 9.864$.

TABLE I. Eigenvalues for marginal Hamiltonians of 2D Henon–Heiles system ($E^{(0)}_{\max}=12.0$). The harmonic $\hat{H}_x$ results are analytical. The $\hat{H}_y$ potential is an altered cubic, with 24 bound states. These were computed to 10^{-10} accuracy, using an $N=1551$ sinc DVR.

	Marginal Hamiltonian eigenvalues	
State index	$\hat{H}_x$ energy (analytical)	$\hat{H}_y$ energy (computed)
1	−1.939 764 130	−1.277 368 110
2	−0.834 718 250	−0.186 647 732
3	0.270 327 628	0.896 555 180
4	1.375 373 510	1.971 984 970
5	2.480 419 380	3.039 364 720
6	3.585 465 260	4.098 393 340
7	4.690 511 140	5.148 742 050
8	5.795 557 020	6.190 050 150
9	6.900 602 900	7.221 919 790
10	8.005 648 780	8.243 909 610
11	9.110 694 650	9.255 526 650
12	10.215 740 500	10.256 216 200
13	11.320 786 400	11.245 348 600
14	12.425 832 300	12.222 201 700
15	13.530 878 200	13.185 937 800
16	14.635 924 000	14.135 570 900
17	15.740 969 900	15.069 920 700
18	16.846 015 800	15.987 543 900
19	17.951 061 700	16.886 627 400
20	19.056 107 600	17.764 810 200
21	20.161 153 400	18.618 862 000
22	21.266 199 300	19.444 019 400
23	22.371 245 200	20.232 303 000
24	23.476 291 100	20.966 243 700

TABLE II. Computed eigenvalues (below $E=E_{\max}=8.3$) for 2D Henon–Heiles system, using the largest PSO DVR ($E_{\text{cut}}=21.5$, $N=528$). Uncertain digits in column II are underlined. The last two columns: error comparison between optimized sinc DVR and PSO DVR of identical size ($N=380$).

Henon–Heiles eigenvalues		Deviations from column II	
State label	PSO DVR energy $N=528$	Sinc DVR error $N=380$	PSO DVR error $N=380$
$1A_1$	0.998 594 772 608	−0.27(−11)	−0.21(−13)
$1E$	1.990 076 760 080	−0.87(−09)	0.94(−13)
$1E$	1.990 076 760 090	0.82(−09)	0.57(−13)
$2A_1$	2.956 242 988 990	−0.15(−08)	0.27(−12)
$2E$	2.985 326 428 070	−0.63(−08)	0.16(−12)
$2E$	2.985 326 428 070	0.47(−08)	0.12(−12)
$3E$	3.925 963 721 090	0.33(−07)	0.50(−11)
$3E$	3.925 963 721 090	1.00(−07)	0.21(−10)
$3A_1$	3.982 417 283 280	−0.47(−07)	0.98(−11)
$1A_2$	3.985 760 926 080	1.00(−07)	0.67(−12)
$4A_1$	4.870 144 005 490	−0.92(−06)	0.65(−09)
$4E$	4.898 644 204 450	−0.16(−05)	0.38(−09)
$4E$	4.898 644 204 460	0.36(−06)	0.58(−09)
$5E$	4.986 251 014 940	−0.10(−05)	0.13(−10)
$5E$	4.986 251 014 950	0.57(−06)	0.25(−09)
$6E$	5.817 019 099 880	0.33(−05)	0.73(−08)
$6E$	5.817 019 100 430	0.83(−05)	0.31(−07)
$5A_1$	5.867 014 809 650	0.74(−06)	0.21(−07)
$2A_2$	5.881 446 098 760	0.44(−05)	0.16(−08)
$7E$	5.991 326 955 770	−0.44(−05)	0.18(−08)
$7E$	5.991 326 955 790	0.47(−05)	0.37(−08)
$6A_1$	6.737 916 244 810	−0.21(−04)	0.48(−06)
$8E$	6.764 866 571 950	−0.35(−04)	0.32(−06)
$8E$	6.764 866 580 150	0.15(−04)	0.55(−06)
$9E$	6.853 430 627 710	−0.32(−04)	0.12(−07)
$9E$	6.853 430 634 960	0.27(−04)	0.26(−06)
$3A_2$	6.998 931 928 770	0.30(−04)	0.26(−07)
$7A_1$	6.999 386 910 290	−0.27(−04)	0.60(−07)
$10E$	7.659 485 640 670	−0.86(−04)	0.33(−05)
$10E$	7.659 486 027 880	0.44(−04)	0.13(−04)
$8A_1$	7.697 721 758 120	−0.12(−03)	0.97(−05)
$4A_2$	7.736 884 760 380	0.31(−04)	0.88(−06)
$11E$	7.832 735 235 730	−0.16(−03)	0.95(−06)
$11E$	7.832 735 281 080	0.84(−04)	0.27(−05)
$12E$	8.009 424 777 490	−0.15(−03)	0.12(−06)
$12E$	8.009 424 815 660	0.12(−03)	0.91(−06)

The DPB, obtained from the marginal quantum Hamiltonians associated with Eq. (5.4), is truncated by comparing the marginal eigenvalues against E_{cut}. Consequently, it is necessary to determine the eigenvalues of the $\hat{H}_x$ and $\hat{H}_y$ operators, as well as their eigenfunctions. In the simple harmonic case of $\hat{H}_x$, these are known analytically. The $\hat{H}_y$ case is somewhat more complicated—not only because the eigenproblem must be solved numerically, but also because of the decreasing potential for $y>y_0$. The latter implies that $\hat{H}_y$, like $\hat{H}$ itself, has no true bound states. In order to obtain a bound state basis, we have altered the potential slightly by setting $V_y(y)=V_y(y_0)$ for $y>y_0$.

For the lower energy states, this alteration has almost no effect. Even for states near $E^{(0)}_{\max}=12.0$, the tunneling is almost negligible; despite the proximity to E_{dis}, the $V_y(y)$ potential well is almost 25 units deep [Fig. 6(b)]. As E_{cut} approaches $V_y(y_0)$ however, there is of course pronounced tunneling, which is ignored by our approximation. In this limit however, these additional states are used only to lend additional accuracy to the DVR calculation, since the maximum energy of interest $E_{\max}$ is necessarily below E_{dis}. Consequently, the tunneling discrepancy for states with energies near $V_y(y_0)$ is probably not significantly detrimental to the calculation.

Far more significant is the fact that the altered potential in y has only a finite number of bound states—24 in all. The largest possible basis size is therefore limited. However, the situation is much better than for $H^{(0)}_y$, for which the ten bound states would only just reach $E^{(0)}_{\max}$. This would be insufficient for obtaining accurate DVR results for the higher energies in the desired range; whereas the basis obtained from the first-order calculation of $\hat{V}_y$ turns out to yield very reasonable accuracy, as is discussed in Sec. V D.

In any event, using a 1D sinc DVR with 1551 points, we have calculated the eigenfunctions and eigenvalues of the 24 bound states of the altered $\hat{H}_y$ operator to an accuracy of at least 10^{-10}. The converged $\hat{H}_y$—and analytical $\hat{H}_x$—eigenvalues are presented in Table I. The same truncation energy $E_{\text{cut}}>E_{\max}$ is used to limit both marginal basis sets. The PSO DVR constructed from the resultant DPB is therefore customized for an eigenvalue calculation of $\hat{H}$ for energies up to the maximum value of interest $E_{\max}$.

There is a slight ambiguity pertaining to the precise value of $E_{\max}$ that should be taken in this regard. Technically, the value $E^{(0)}_{\max}=12.0$ is only a zeroth-order approximation to $E_{\max}$, which can change with successive iterations

TABLE III. Comparison of errors of computed eigenvalues (below $E=9.3$) for 2D Henon–Heiles system, for rectangular PSO DVRs of increasing basis truncation energy $E_{\rm cut}$. Errors are deviations with respect to the energies of Table II column II ($N=528$ PSO DVR). The horizontal line near the bottom denotes the maximum energy of interest, $E_{\rm max}=8.3$.

Convergence errors vs $E_{\rm cut}$ for Henon–Heiles system				
$E_{\rm cut}=8.5$ ($N=100$)	$E_{\rm cut}=12.0$ ($N=169$)	$E_{\rm cut}=15.0$ ($N=256$)	$E_{\rm cut}=18.0$ ($N=380$)	$E_{\rm cut}=20.0$ ($N=440$)
0.14(−09)	0.42(−12)	0.89(−15)	-0.21(−13)	0.35(−13)
0.81(−08)	0.14(−10)	0.18(−12)	0.94(−13)	0.79(−13)
0.16(−07)	0.67(−10)	0.45(−12)	0.57(−13)	0.53(−13)
0.94(−06)	0.33(−08)	0.24(−10)	0.27(−12)	0.12(−12)
0.28(−06)	0.16(−08)	0.11(−10)	0.16(−12)	0.34(−13)
0.74(−06)	0.18(−08)	0.15(−10)	0.12(−12)	0.79(−13)
0.22(−04)	0.40(−07)	0.39(−09)	0.50(−11)	0.11(−11)
0.49(−04)	0.18(−06)	0.19(−08)	0.21(−10)	0.49(−11)
0.25(−04)	0.77(−07)	0.78(−09)	0.98(−11)	0.22(−11)
0.19(−05)	0.10(−07)	0.76(−10)	0.67(−12)	0.14(−12)
0.91(−03)	0.34(−05)	0.42(−07)	0.65(−09)	0.15(−09)
0.18(−03)	0.25(−05)	0.26(−07)	0.38(−09)	0.89(−10)
0.12(−02)	0.25(−05)	0.37(−07)	0.58(−09)	0.15(−09)
0.96(−04)	0.15(−06)	0.68(−09)	0.13(−10)	0.33(−11)
0.26(−03)	0.12(−05)	0.17(−07)	0.25(−09)	0.61(−10)
0.42(−02)	0.37(−04)	0.34(−06)	0.73(−08)	0.19(−08)
0.14(−01)	0.85(−04)	0.16(−05)	0.31(−07)	0.83(−08)
0.13(−01)	0.62(−04)	0.10(−05)	0.21(−07)	0.54(−08)
1.00(−03)	0.89(−05)	0.12(−06)	0.16(−08)	0.37(−09)
0.34(−03)	0.28(−05)	0.71(−07)	0.18(−08)	0.50(−09)
0.25(−02)	0.14(−04)	0.20(−06)	0.37(−08)	0.92(−09)
0.35(−01)	0.94(−03)	0.18(−04)	0.48(−06)	0.13(−06)
0.15(−01)	0.61(−03)	0.13(−04)	0.32(−06)	0.88(−07)
0.72(−01)	0.10(−02)	0.20(−04)	0.55(−06)	0.16(−06)
0.14(−01)	0.20(−03)	0.70(−06)	0.12(−07)	0.34(−08)
0.75(−01)	0.33(−03)	0.99(−05)	0.26(−06)	0.74(−07)
0.46(−02)	0.61(−04)	0.13(−05)	0.26(−07)	0.67(−08)
0.13(−01)	0.96(−04)	0.18(−05)	0.60(−07)	0.17(−07)
0.79(−01)	0.76(−02)	0.88(−04)	0.33(−05)	0.10(−05)
0.80(−01)	0.95(−02)	0.36(−03)	0.13(−04)	0.41(−05)
0.13(00)	0.10(−01)	0.25(−03)	0.97(−05)	0.30(−05)
0.12(00)	0.14(−02)	0.37(−04)	0.88(−06)	0.24(−06)
0.56(−01)	0.57(−03)	0.21(−04)	0.95(−06)	0.32(−06)
0.18(00)	0.34(−02)	0.80(−04)	0.27(−05)	0.79(−06)
0.19(−01)	0.38(−03)	0.66(−05)	0.12(−06)	0.31(−07)
0.22(00)	0.62(−03)	0.21(−04)	0.91(−06)	0.30(−06)
0.15(00)	0.42(−01)	0.20(−02)	0.11(−03)	0.36(−04)
0.14(00)	0.26(−01)	0.17(−02)	0.73(−04)	0.24(−04)
0.30(00)	0.75(−01)	0.26(−02)	0.15(−03)	0.52(−04)
0.23(00)	0.14(−01)	0.29(−03)	0.62(−05)	0.17(−05)
0.31(00)	0.26(−01)	0.84(−03)	0.44(−04)	0.15(−04)
0.19(00)	0.82(−02)	0.36(−03)	0.14(−04)	0.44(−05)
0.23(00)	0.11(−01)	0.33(−03)	0.20(−04)	0.73(−05)
0.11(00)	0.17(−02)	0.49(−04)	0.23(−05)	0.82(−06)
0.65(00)	0.25(−02)	0.14(−03)	0.78(−05)	0.27(−05)

(Sec. III C). To be consistent, we should use the first-order $E_{\rm max}$, defined quasiclassically as the contours of $H_x^{(1)}(x,p_x)$ and $H_y^{(1)}(y,p_y)$ for which the volume of $\mathcal{R}^{(1)}$ equals that of $\mathcal{R}^{(0)}$, i.e., $\mathcal{V}$. The quantum procedure is even more straightforward—simply adjust $E_{\rm max}$ until the truncated basis size is closest to $\mathcal{V}/(2\pi)^n$. This basis size is approximately 94, which—from Table I—is found to yield $E_{\rm max}=E_{\rm max}^{(1)}\approx 8.3$.

D. Results: PSO DVR eigenvalues

Using the PSO DVR constructed from the DPB described in Sec. V C, we have performed eigenvalue calculations of the Henon–Heiles system. A variety of $E_{\rm cut}$ truncations were used, starting near the first-order $E_{\rm max}$ value ($E_{\rm cut}=8.5$), and working up to $E_{\rm cut}=21.5$, which yields all 24 of the *y*-coordinate bound states. Results are presented in Tables II and III. Since $E_{\rm cut}$ is the only convergence parameter, we use the results of the largest DVR grid ($E_{\rm cut}=21.5$, $N=22\times 24=528$) as the reference for the errors in Table III.

The last column of Table III provides an indication of the converged accuracy of these eigenvalues, which are presented in Table II. Another indication is the numerical difference between the two eigenvalues of the theoretically degenerate pairs of E symmetry. Since we have not exploited this symmetry in the PSO DVR computation, both eigenvalues of each pair are calculated explicitly. In determining the significant figures of the second column of Table II, we use the *larger* of the two error measures. We regard any accuracy beyond $\sim 10^{-9}$ as suspect however, due to the quasibound nature of the Henon–Heiles system (Sec. V A). Our results fall within the error bars of previous calculations,[44–48] for energies below $E_{\rm max}$.

Perhaps the most striking feature of Table III is the extremely sudden loss of accuracy that occurs as one crosses over the $E_{\rm max}\approx 8.3$ threshold. In all of the grids considered, one finds a sudden two-order-of-magnitude error increase between the $E\approx 8.01$ and $E\approx 8.55$ eigenvalues. Although a general loss of accuracy was expected, the abruptness of the transition is quite surprising, and definitely much more extreme than what we had anticipated. It is reassuring to find that the transition energy does not vary at all with increasing basis size—suggesting that the PSO DVR method really does decouple the energy range from the basis size. On the other hand, even within the range of interest the error tends to increase with increasing energy, as is—to our knowledge—true of all other DVR schemes to date. Moreover, there are certain large aberrations well below $E_{\rm max}$.

On the whole though, the PSO DVR appears to be quite efficient. Even with as few as 380 points, the error of the largest of the 36 energies below $E_{\rm max}$ is only about one part in 10^7. This should be contrasted with the results of a 2D sinc DVR calculation, which we have also applied to the Henon–Heiles system. In the latter, potential energy truncation of the grid was performed to reduce its size. The grid spacing (0.6) and potential cutoff energy (17.0) were optimized with respect to the accuracy of the eigenenergies in range. Nevertheless, the sinc DVR errors are several orders of magnitude larger than those of a PSO DVR of identical size ($N=380$). A direct comparison for each of the 36 desired eigenvalues is given in the last two columns of Table II.

The preceding PSO DVR results were all obtained using rectangular DVR grids, with the same number of grid points as basis functions. In principle, one can discard grid points from areas where the potential energy is substantially larger than $E_{\rm max}$, so as to reduce the size of the DVR matrix representing the Hamiltonian. This truncation procedure is often

TABLE IV. Comparison of errors of computed eigenvalues (below $E=E_{max}=8.3$) for 2D Henon–Heiles system, for truncated PSO DVR grids of increasing potential cutoff energy V_{cut}. Untruncated grid is the $N=380$ PSO DVR of Tables II/III column IV. Errors are with respect to Table II column II.

Convergence errors vs V_{cut} for Henon–Heiles system			
$V_{cut}=10.0$ ($N=247$)	$V_{cut}=14.0$ ($N=309$)	$V_{cut}=18.0$ ($N=348$)	$V_{cut}=24.0$ ($N=364$)
0.13(−06)	0.29(−09)	0.11(−11)	0.81(−14)
0.12(−05)	0.43(−08)	0.14(−10)	0.80(−13)
0.22(−05)	0.51(−08)	0.28(−10)	0.58(−13)
0.19(−04)	0.65(−07)	0.33(−09)	0.40(−12)
0.11(−04)	0.14(−07)	0.11(−09)	0.26(−12)
0.14(−04)	0.71(−07)	0.33(−09)	0.18(−12)
0.10(−03)	0.41(−06)	0.19(−08)	0.57(−11)
0.14(−03)	0.61(−06)	0.41(−08)	0.23(−10)
0.71(−04)	0.29(−06)	0.24(−08)	0.11(−10)
0.68(−04)	0.27(−06)	0.95(−09)	0.63(−12)
0.69(−03)	0.35(−05)	0.25(−07)	0.66(−09)
0.49(−03)	0.14(−05)	0.11(−07)	0.38(−09)
0.65(−03)	0.44(−05)	0.32(−07)	0.60(−09)
0.24(−03)	0.44(−06)	0.82(−08)	0.16(−10)
0.36(−03)	0.25(−05)	0.11(−07)	0.25(−09)
0.26(−02)	0.13(−04)	0.99(−07)	0.74(−08)
0.30(−02)	0.22(−04)	0.23(−06)	0.31(−07)
0.19(−02)	0.14(−04)	0.17(−06)	0.21(−07)
0.23(−02)	0.12(−04)	0.60(−07)	0.16(−08)
0.10(−02)	0.39(−05)	0.41(−07)	0.18(−08)
0.11(−02)	0.91(−05)	0.62(−07)	0.37(−08)
0.98(−02)	0.79(−04)	0.13(−05)	0.48(−06)
0.73(−02)	0.42(−04)	0.67(−06)	0.32(−06)
0.10(−01)	0.10(−03)	0.17(−05)	0.55(−06)
0.63(−02)	0.26(−04)	0.46(−06)	0.12(−07)
0.75(−02)	0.76(−04)	0.62(−06)	0.26(−06)
0.30(−02)	0.32(−04)	0.27(−06)	0.26(−07)
0.38(−02)	0.19(−04)	0.25(−06)	0.60(−07)
0.25(−01)	0.23(−03)	0.54(−05)	0.33(−05)
0.28(−01)	0.36(−03)	0.18(−04)	0.13(−04)
0.21(−01)	0.26(−03)	0.14(−04)	0.97(−05)
0.28(−01)	0.24(−03)	0.24(−05)	0.88(−06)
0.17(−01)	0.12(−03)	0.25(−05)	0.95(−06)
0.20(−01)	0.23(−03)	0.43(−05)	0.27(−05)
0.86(−02)	0.60(−04)	0.13(−05)	0.12(−06)
0.99(−02)	0.11(−03)	0.14(−05)	0.91(−06)

applied to sinc DVR grids,[8] although its use has been discouraged[13]—particularly for PO DVRs, for which a part of the potential function has already been used to define the basis.[47] Nevertheless, in the remainder of this section, we examine the consequences of applying a potential energy truncation scheme to the PSO DVR grids.

A DVR point (i,j) is discarded if and only if $V(x_i,y_j)>V_{cut}$, with V_{cut} itself sufficiently larger than E_{max}. It is convenient to write the potential function as $V(x,y)=V_x(x)+V_y(y)+\Delta(x,y)$. In the limit of small Δ, it is clear that for $V_{cut}>E_{cut}$, the accuracy of the desired eigenvalues will not be significantly worse than that of the corresponding rectangular grid. This accuracy may diminish exponentially however, as V_{cut} is decreased below E_{cut}. In reality of course, $\Delta(x,y)$ is generally not negligible; nevertheless, the PSO residual is known to have the smallest possible (averaged) square magnitude, and an average value of zero. Consequently, although the sudden transition of accuracy versus V_{cut} near $V_{cut}=E_{cut}$ should be smoothed out somewhat due to Δ, we still expect there to be a minimal V_{cut} value—larger than, but on the same order as, E_{cut}—above which the accuracy should be comparable to that of the rectangular grid.

We have tested this idea on the 19×20 Henon–Heiles PSO DVR grid, corresponding to $E_{cut}=18.0$. Because the potential is not very separable, $\Delta(x,y)$—though minimized—is not very small. Nevertheless, the eigenvalue errors for the various V_{cut} values presented in Table IV (10.0, 14.0, 18.0, and 24.0) seem to bear out our expectations. Although the $N=348$ grid of $V_{cut}=18.0$ (Fig. 5) is one or two orders of magnitude less accurate than the $N=380$ rectangular grid (Tables II and III, column IV), the $N=364$ results ($V_{cut}=24.0$) are virtually indistinguishable from the latter. As expected, the error increases quite rapidly below $V_{cut}=18.0$.

The practical question however, is whether potential energy truncation is more efficient than simply using a smaller rectangular grid. Upon comparing Tables III and IV, this appears unlikely for all V_{cut} values considered except $V_{cut}=24.0$, for which the grid size is reduced by only about 5%. For the Henon–Heiles application therefore, potential energy truncation does not appear to accomplish very much. Although this is anticipated for many applications, there are some situations for which potential energy truncation may indeed be useful. If there are more than just a few degrees of freedom, for example, then grid truncation may be quite effective, as the multiplicative effect of shaving a small percentage of points per degree of freedom can accumulate into something quite substantial.

VI. SUMMARY AND CONCLUSIONS

The idea of tailoring a representation to a particular system of interest is an important one, regardless of the specific application or computational method. The difficulty however, is that an exact optimization may be more challenging than the original problem itself. Thirteen years ago, one of the authors (J.C.L.) summed up the situation as follows:[47] ''The question of the best *a priori* basis for a specific problem is one that cannot be answered in general, since it depends on the number of eigenvalues required, the accuracy to which they are required, and the potential for which they are required.'' Nevertheless, in the present work, we believe we have found the answer to precisely this question—at least for the important special case of direct-product representations.

This is accomplished via an optimal separable basis theory[4] generalized to incorporate Hamiltonian projections (Sec. II A)—although this was not evident when we first established Eq. (2.8). In any event, an equally essential component is the relation between the truncated basis operator $\hat{\rho}_N$, and its quasiclassical analog, the Thomas–Fermi distribution.[18–20] It is the quantitative similarity of the phase space representations of these two entities that enables us to obtain a nearly optimal solution by merely evaluating a few simple integrals. Moreover, the accuracy of this correspondence increases with the basis size N. It is encouraging that the method becomes better in precisely the limit in which the problem becomes difficult.

It should be mentioned that strong separability, although

a necessary prerequisite for conventional DVR applications (Sec. II C), introduces its own inherent limitations. The direct-product constraint is decidedly severe, especially if there are many degrees of freedom. It greatly limits the maximum possible efficiency of the resultant basis, for instance, so that we still expect the number of required basis functions (or DVR points) N to be much larger than the number of accurate eigenvalues K. On the other hand, we can probably deviate slightly from the true optimum—as in the quasiclassical solution of Eq. (3.8), or even its first-order approximation—without reducing the efficiency very much. An additional limitation of the direct-product constraint—even for the exact quantum solution—is that the efficiency may vary significantly with the choice of coordinates.

The important question is, however: in comparison with other methods, how much is the efficiency expected to improve? We believe that in general the improvement will be very significant—at least for eigenvalue calculations of typical polyatomic systems. One indication of this can be found in the ''wasted phase space'' picture of Sec. II C and Fig. 1(b). One can think of the optimized sinc DVR region $\mathcal{R}_{\text{sinc}}$ as a separable product of regions on each of the $2n$ *phase space* coordinates. There are thus a total of $2n$ constraints of separability, as opposed to the PSO result of this paper, which has only n such constraints. We therefore expect the respective efficiencies to be given approximately by μ^{2n} and μ^n, with $0<\mu<1$, resulting in $N_{\text{PSO}}\approx\mu^n N_{\text{sinc}}$.

Another, more concrete indication of this improvement however, can be found in the last two columns of Table II. Here we find the accuracy of a PSO vs sinc DVR calculation of a given size improved by two to four orders of magnitude. Note that according to the argument just presented, the efficiency *improvement* should be greater for higher dimensionalities. This improvement should not be affected much by the separability of the Hamiltonian, although separability should have a great effect on the efficiency itself. Thus, the high degree of nonseparability of the Henon–Heiles potential in the relevant energy range is reflected in the fact that $N\approx 10$ K in order to achieve a competitive level of accuracy. Incidentally, the fact that all but one of the convergence errors in Table III are *positive* suggests that the quadrature error is much smaller than the representational error, in accord with Sec. III D.

We foresee many possible avenues for future exploration, both with and without the constraint of separability. It might be worthwhile, for instance, to apply the present method to angular coordinates and nonorthogonal kinetic energies, as arise when rotational symmetry is applied to molecular systems. It could also be useful to examine the question of coordinate choice more carefully. An optimization of coordinates with respect to Hamiltonian separability might improve the efficiency dramatically[50]—perhaps even resulting in accurate eigenvalues above E_{cut}. Ideally, one would like to generalize the PSO formalism to optimize both the coordinates and the basis functions simultaneously. A similar approach has already been developed for the VSCF method, for example.[51]

In nondirect-product applications, it is the Thomas–Fermi density proper, i.e., the $\rho^q(q_1,\ldots,q_n)$ of Eq. (2.11), which is anticipated to be most useful. Since this can be interpreted as the density of DVR points in configuration space, it could serve as a very useful guide for a generalized nondirect-product DVR, or even a distributed Gaussian basis (DGB),[47] treatment. These approaches are exempt from the direct-product limitations of the present method, and might potentially require N to be only slightly larger than K, at least in principle. A final comment: Since a basis/DVR is the end result of phase space optimization, the procedure may be used in conjunction with any other application where a basis/DVR is appropriate. These might include: Lanczos diagonalization,[52,53] successive truncation and diagonalization,[3,10] and scattering applications such as Green's function evaluation, optimized preconditioning,[27] etc.

ACKNOWLEDGMENTS

This work was supported, in part, by the National Science Foundation under Grant. No. CHE-9634440.

APPENDIX: SELF-CONSISTENCY OF THE OPTIMAL SOLUTION

In this appendix, we derive a self-consistency relation for the direct-product quasiclassical UME of Eq. (3.4) that satisfies the stationarity condition of Eq. (2.12). The $2n$-dimensional UME density $\rho(q_1,p_1,\ldots,q_n,p_n)$ is a product of n two-dimensional UME densities $\rho_k(q_k,p_k)$, which are essentially arbitrary. However, there is an overall constraint that the total phase space volume enclosed by $\mathcal{R}$ must remain fixed.

The region $\mathcal{R}_k$, on the kth marginal phase space is uniquely determined by the curves that define its boundaries, together with a specification of orientedness (i.e., ''inside'' versus ''outside''). The curves themselves can be given as momentum functions of position $p_k^{\text{ext}}(q_k)$, as is done in Wentzel–Kramers–Brillouin (WKB) or Hamilton–Jacobi theory. The $p_k^{\text{ext}}(q_k)$ functions are necessarily multivalued, if they are to describe closed regions (Fig. 3). In the $T+V$ case for instance, there are two such curves, symmetrically situated about the q_k axis. It would therefore be more accurate to label the single-valued branches with an additional index, such as $p_{k\,(\alpha)}^{\text{ext}}(q_k)$. We can legitimately suppress this index however, as the argument can be applied—without significant modification—to each branch independently.

Let the $p_k^{\text{ext}}(q_k)$ be chosen so as to satisfy Eq. (2.12), for a given total phase space volume $\mathcal{V}$. The integral of Eq. (2.12) can be rewritten in terms of the $p_k^{\text{ext}}(q_k)$ as

$$\int \int_{p_n^{\text{ext}}(q_n)^-}^{p_n^{\text{ext}}(q_n)^+} \cdots \int \int_{p_1^{\text{ext}}(q_1)^-}^{p_1^{\text{ext}}(q_1)^+} H(q_1,p_1,\ldots,q_n,p_n) \times dp_1\,dq_1\cdots dp_n\,dq_n, \tag{A1}$$

where the plus and minus signs in the limits of integration denote the orientedness of the branches. Small variations to the regions $\mathcal{R}_k$ are identified with the addition of small deviation functions $\varepsilon_k(q_k)$ to the $p_k^{\text{ext}}(q_k)$. Stationarity of the functional implies that the integrated value of Eq. (A1) re-

mains constant, to first order in the $\varepsilon_k(q_k)$'s, for all variations of the latter that preserve the total phase space volume $\mathcal{V}$.

We need consider only those variations for which any two of the n ε's are nonzero (labeled j and k). The fixed-$\mathcal{V}$ constraint implies that

$$\mathcal{A}_j \int \pm \varepsilon_k(q_k)\, dq_k + \mathcal{A}_k \int \pm \varepsilon_j(q_j)\, dq_j = 0 \tag{A2}$$

(integration limits suppressed), where $\mathcal{A}_k$ is the marginal area of the region $\mathcal{R}_k$, etc. (Sec. III B), and the plus or minus sign again reflects orientedness. Stationarity of Eq. (A1) on the other hand, requires that

$$\int \pm \varepsilon_k(q_k) \left\{ \int H(p_k = p_k^{\mathrm{ext}}(q_k)) \prod_{i \neq k} dq_i\, dp_i \right\} dq_k + \int \pm \varepsilon_j(q_j) \left\{ \int H(p_j = p_j^{\mathrm{ext}}(q_j)) \prod_{i \neq j} dq_i\, dp_i \right\} dq_j = 0. \tag{A3}$$

The inner integrals in Eq. (A3) resemble the marginal Hamiltonian expressions of OSB theory [Eq. (3.5), first line]. Rewriting Eq. (A3) in terms of the latter, we find

$$\mathcal{A}_j \int \pm \varepsilon_k(q_k)\, H_k(q_k, p_k^{\mathrm{ext}}(q_k))\, dq_k + \mathcal{A}_k \int \pm \varepsilon_j(q_j)\, H_j(q_j, p_j^{\mathrm{ext}}(q_j))\, dq_j = 0, \tag{A4}$$

where Eq. (A2) has been used implicitly to cancel the E_0 constant terms.

Equation (A4) must hold for all variations of $\varepsilon_j(q_j)$ and $\varepsilon_k(q_k)$. If $\varepsilon_j(q_j) = 0$, then the first term alone must be zero for all variations $\varepsilon_k(q_k)$, implying that $H_k(q_k, p_k^{\mathrm{ext}}(q_k))$ is a *constant*, denoted by E_k. The optimal regions $\mathcal{R}_k$ are thus given by $H_k(q_k, p_k) < E_k$. By making this substitution into Eq. (A4) and allowing $\varepsilon_j(q_j)$ to be arbitrary, we find

$$E_k \mathcal{A}_j \int \pm \varepsilon_k(q_k)\, dq_k + E_j \mathcal{A}_k \int \pm \varepsilon_j(q_j)\, dq_j = 0. \tag{A5}$$

By virtue of the Eq. (A2) constraint however, this implies that $E_j = E_k \equiv E_{\max}$.

Therefore, the optimal quasiclassical solution satisfies a self-consistency relation vis-a-vis the OSB marginal Hamiltonians: the optimal $\mathcal{R}_k$ are obtained from the optimal $H_k(q_k, p_k)$ via the contours of the latter; *and*, the same $H_k(q_k, p_k)$ are obtained from the same $\mathcal{R}_k$ via OSB theory. Moreover, the maximum energy $E_{\max}$ is the same for each of the n degrees of freedom. These results are summarized in Eq. (3.5).

[1] J. M. Bowman, Acc. Chem. Res. **19**, 202 (1986).
[2] J. M. Bowman, Comput. Phys. Commun., Special Issue on ''Molecular Vibrations,'' **51**, 225 (1988).
[3] Z. Bačić and J. C. Light, Annu. Rev. Phys. Chem. **40**, 469 (1989).
[4] B. Poirier, Phys. Rev. A **56**, 120 (1997).
[5] D. O. Harris, G. G. Engerholm, and W. D. Gwinn, J. Chem. Phys. **43**, 1515 (1965).
[6] A. S. Dickinson and P. R. Certain, J. Chem. Phys. **49**, 4209 (1968).
[7] J. V. Lill, G. A. Parker, and J. C. Light, Chem. Phys. Lett. **89**, 483 (1982).
[8] J. C. Light, I. P. Hamilton, and J. V. Lill, J. Chem. Phys. **82**, 1400 (1985).
[9] J. V. Lill, G. A. Parker, and J. C. Light, J. Chem. Phys. **85**, 900 (1986).
[10] Z. Bačić and J. C. Light, J. Chem. Phys. **85**, 4594 (1986).
[11] J. Echave and D. C. Clary, Chem. Phys. Lett. **190**, 225 (1992).
[12] H. Wei and T. Carrington, Jr., J. Chem. Phys. **97**, 3029 (1992).
[13] M. J. Bramley and T. Carrington, Jr., J. Chem. Phys. **99**, 8519 (1993).
[14] N. M. Poulin *et al.*, J. Chem. Phys. **104**, 7807 (1996).
[15] H. Chen, S. Liu, and J. C. Light, J. Chem. Phys. **110**, 168 (1999).
[16] L. H. Thomas, Proc. Cambridge Philos. Soc. **23**, 542 (1927).
[17] E. Fermi, Z. Phys. **48**, 73 (1928).
[18] D. A. Kirzhnits, Sov. Phys. JETP **5**, 64 (1957).
[19] S. Golden, Rev. Mod. Phys. **32**, 322 (1960).
[20] J. C. Light and J. M. Yuan, J. Chem. Phys. **58**, 660 (1973).
[21] S. Nordholm, J. Chem. Phys. **86**, 363 (1987).
[22] H. Weyl, Z. Phys. **46**, 1 (1928).
[23] E. Wigner, Phys. Rev. **40**, 749 (1932).
[24] J. E. Moyal, Proc. Cambridge Philos. Soc. **45**, 99 (1949).
[25] M. Hillery, R. F. O'Connell, M. O. Scully, and E. P. Wigner, Phys. Lett. **106**, 121 (1984).
[26] J. M. Bowman, J. S. Bittman, and L. B. Harding, J. Chem. Phys. **85**, 911 (1986).
[27] B. Poirier and W. H. Miller, Chem. Phys. Lett. **265**, 77 (1997).
[28] B. Poirier, J. Chem. Phys. **108**, 5216 (1998).
[29] J. P. Foster and F. Weinhold, J. Am. Chem. Soc. **102**, 7211 (1980).
[30] G. C. Carney, L. L. Sprandel, and C. W. Kern, Adv. Chem. Phys. **37**, 305 (1978).
[31] J. M. Bowman, J. Chem. Phys. **68**, 608 (1978).
[32] M. A. Ratner, J. Phys. Chem. **90**, 20 (1986).
[33] E. Fattal, R. Baer, and R. Kosloff, Phys. Rev. E **53**, 1217 (1996).
[34] E. Tiesinga, C. J. Williams, and P. S. Julienne, Phys. Rev. A **57**, 4257 (1998).
[35] Z. Bačić and J. C. Light, J. Chem. Phys. **86**, 3065 (1987).
[36] To avoid confusion, terms like ''1D,'' etc., should be read as ''one degree of freedom;'' whereas the phrase ''one-dimensional'' always refers to just a single coordinate, i.e., q or p, but not both.
[37] C. Lanczos, *The Variational Principle of Mechanics*, 4th ed. (Dover, Mineola, NY, 1986).
[38] M. Faist, J. Chem. Phys. **65**, 5427 (1976).
[39] The shadow region is really just the projection of $\mathcal{R}^{\mathrm{un}}$ on to the marginal phase space. We use the term ''shadow'' however, to avoid confusion with ''projection'' in the sense of Eq. (2.6).
[40] D. Hartree, Proc. Cambridge Philos. Soc. **24**, 89 (1928).
[41] V. Fock, Z. Phys. **61**, 126 (1930).
[42] E. H. Lieb and B. Simon, in *The Stability of Matter: From Atoms to Stars*, edited by W. Thirring (Springer, New York, 1997), Chap. 4, pp. 299–308.
[43] W. H. Press *et al.*, in *Numerical Recipes*, 1st ed. (Cambridge University Press, Cambridge, 1989), pp. 126–130.
[44] D. W. Noid and R. A. Marcus, J. Chem. Phys. **62**, 2119 (1976).
[45] M. J. Davis and E. J. Heller, J. Chem. Phys. **71**, 3383 (1979).
[46] G. Hose and H. S. Taylor, J. Chem. Phys. **76**, 5356 (1982).
[47] I. P. Hamilton and J. C. Light, J. Chem. Phys. **84**, 306 (1986).
[48] D. S. Zhang, G. W. Wei, D. J. Kouri, and D. K. Hoffman, J. Chem. Phys. **106**, 5216 (1997).
[49] A. N. Drozdov and S. Hayashi, J. Chem. Phys. **110**, 1888 (1999).
[50] J. M. Bowman, J. Zûñiga, and A. Wierzbicki, J. Chem. Phys. **90**, 2708 (1989).
[51] T. C. Thompson and D. G. Truhlar, J. Chem. Phys. **77**, 3031 (1982).
[52] C. Lanczos, J. Res. Natl. Bur. Stand. **45**, 255 (1950).
[53] J. K. Cullum and R. A. Willoughby, *Lanczos Algorithms for Large Symmetric Eigenvalue Computations* (Burkhauser, Boston, MA, 1985).